

## Decoupling Fluorescence and Photochromism in Bifunctional Azo Derivatives for Bulk Emissive Structures

Aurélie Jacquot,<sup>[c]</sup> René M. Williams,<sup>[b]</sup> Albert M. Brouwer,<sup>[b]</sup> and Eléna Ishow\*<sup>[a, c]</sup>

**Abstract:** Bifunctional molecules that combine independent push–pull fluorophores and azo photochromes have been synthesized to create fluorescent structures upon light-induced migration in neat thin films. Their photochromic and emissive properties have been systematically investigated and interpreted in light of those of the corresponding model compounds. Fluorescence lifetimes and photoisomerization and

fluorescence quantum yields have been determined in toluene solution. Kinetic analyses of the femtosecond transient absorption spectra reveal that the fluorophores evolve in a few picoseconds into a distorted intramolecular charge-

transfer excited state, strongly stabilized in energy. Radiative relaxation to the ground state occurred competitively with the energy-transfer process to the azo moiety. Introduction of a 10 Å-long rigid and nonconjugated bridge between the photoactive units efficiently inhibits the energy transfer while it imparts enhanced free volume, which favors photoactivated molecular migration in the solid state.

**Keywords:** azo compounds • fluorescence • laser spectroscopy • photochromism • thin films

### Introduction

Azo-functional derivatives have acquired an indisputable place as photoactivable systems to switch magnetic,<sup>[1–5]</sup> electrical,<sup>[6–10]</sup> and optical dichroic<sup>[11–15]</sup> properties in solution and in the solid state. Light absorption causes photoisomerization from the more stable *E* isomer to the *Z* configuration,<sup>[16]</sup> which is accompanied by dramatic changes in geometry, especially in packed systems such as liquid-crystalline polymers<sup>[17]</sup> or self-assembled monolayers.<sup>[6,18]</sup> The resulting photomechanical effects have been successfully exploited to bend<sup>[19,20]</sup> or rotate<sup>[21]</sup> azo assemblies, free fluorescent drugs entrapped in silica nanocontainers,<sup>[22,23]</sup> or open protein ion channels.<sup>[24]</sup> Among all the possible signals to be modulated, fluorescence emission has, however, rarely been considered,<sup>[25,26]</sup> especially in the solid state.<sup>[27]</sup> Generally, intrinsic fluorescence in simple azo derivatives comes at the expense

of photochromism since both processes correspond to competitive relaxation of the excited states involved. A few examples in the literature report highly fluorescent azo derivatives in which photochromic properties are inhibited through chromophore aggregation<sup>[28,29]</sup> or N=N double-bond coordination to boron atoms.<sup>[30,31]</sup> By contrast, azo units have been grafted onto molecular beacons to sense the pairing of DNA strands upon fluorescence quenching of a fluorophore placed at the extremity of the second complementary strand.<sup>[32]</sup> This involves efficient Förster resonant energy transfer, which operates at a close distance.<sup>[33,34]</sup> Such efficiency stems from the ultrafast azo photoisomerization process, which traps any incoming energy and converts it into radiationless vibrational or photochemical processes.<sup>[35,36]</sup> Avoiding fluorescence quenching by azo units requires multiple spectral and structural issues to be considered. First, the emission of the fluorophore needs to be red shifted with regard to the azo absorption band. Second, the bridge that links the fluorescent and photochromic units must prevent deleterious folding and should suppress energy transfer through bonds or through space. Following these lines, we synthesized in the past bifunctional molecules made of a red light-emitting squaraine unit covalently linked to a push–pull Disperse Red 1-like azo moiety.<sup>[37,38]</sup> Nevertheless, the emission quantum yield ( $\Phi_f$ ) was severely reduced by 60–90% relative to the azo-free squaraine value  $\Phi_f=0.9$ . Formation of weakly emissive states was presumed due to the  $\pi$  stacking of the azo and squaraine aromatic rings permitted by the short ethylene linker.<sup>[39]</sup> This prompted us to replace the squaraine unit with a bulky fluorescent chromophore, known to emit as non-doped material, and mostly absorbing in a region of minimum absorption by the azo unit for selective excitation.<sup>[40]</sup> Additionally, introduction of a long and rigid spacer between the fluorescent and photochromic unit

[a] Prof. E. Ishow  
CEISAM-UMR CNRS 6230  
Université de Nantes, 2 rue de la Houssinière  
44 322 Nantes cedex (France)  
Fax: (+33)2-5112-5402  
E-mail: elena.ishow@univ-nantes.fr

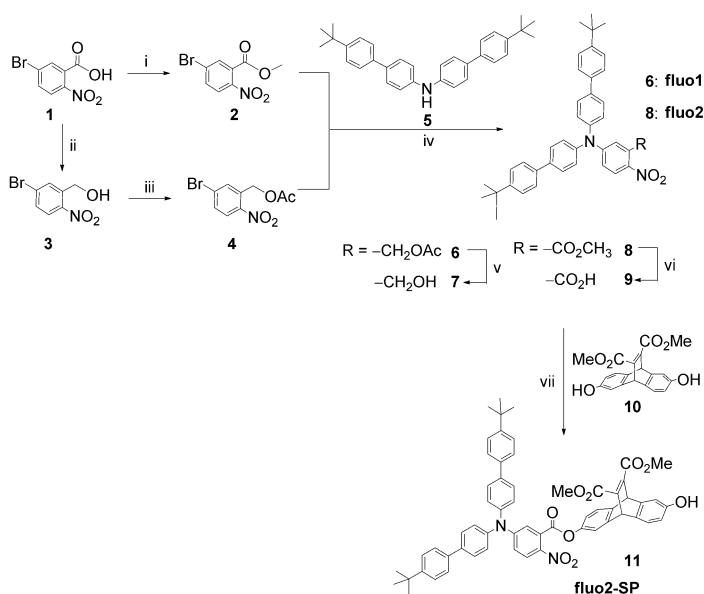
[b] Dr. R. M. Williams, Prof. A. M. Brouwer  
Van't Hoff Institute for Molecular Sciences  
University of Amsterdam, Postbus 94157  
1090 GD Amsterdam (The Netherlands)

[c] Dr. A. Jacquot, Prof. E. Ishow  
PPSM-UMR CNRS 8531  
ENS Cachan  
61 avenue du Président Wilson  
94235 Cachan cedex (France)

Supporting information for this article is available on the WWW under <http://dx.doi.org/10.1002/chem.201103411>.

avoids structural  $\pi$ - $\pi$  stacking and emission quenching by energy transfer.

In the present work, we show that emission from the targeted fluorophores implies picosecond competition between the formation of a distorted radiative excited state and the process of energy transfer to the azo unit. Ultrafast transient absorption spectroscopy measurements reveal that the presence of a 10 Å-long spacer considerably reduces the energy-transfer rate at the sole benefit of the fluorophore emission. Photochromic kinetic studies performed in the ground state show that the azo photoisomerization quantum yields and thermal back-reaction rate constants are little affected by the bridge. This bridge, however, exerts remarkable mechanical properties as evidenced through the fabrication of less dense thin films amenable to enhanced photoinduced surface deformation. The results reported in these studies represent the first comprehensive investigations of fluorescence quenching by azo units by resorting to ultrafast transient absorption spectroscopy and systematically comparing synthetic bifunctional systems with their corresponding monofunctional models. They open new avenues to the design of fluorescent photoswitchable molecules for tracking photomechanically-activated single systems, and provide insight into the efficiency of azo bulk photomigration, subject to lose microscopic surroundings.

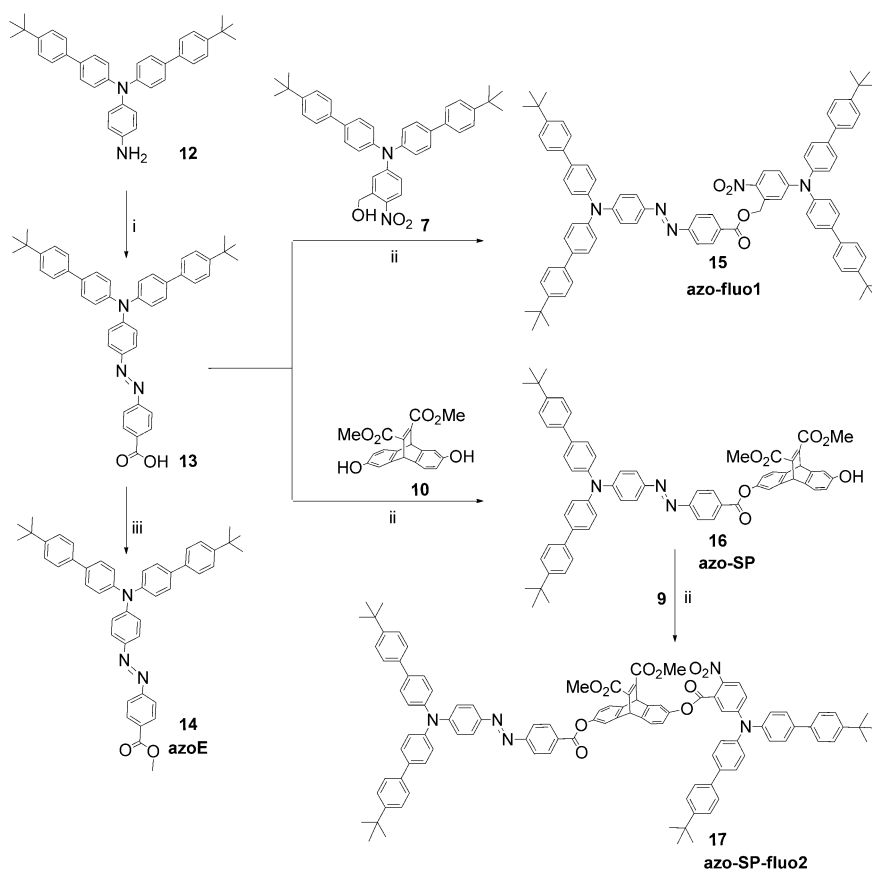


Scheme 1. Synthetic pathway to the formation of fluorescent compounds. i) Thionyl chloride, methanol, pyridine, 0°C, 4 h; ii)  $\text{BH}_3$ -THF, THF, RT, 72 h; iii) acetic anhydride,  $\text{I}_2$ (cat), RT, 30 min; iv)  $\text{Pd}(\text{OAc})_2$ , diphenylphosphineferrocene,  $\text{Cs}_2\text{CO}_3$ , dry toluene, 80°C, 20 h; v)  $\text{NaOH}_{(\text{aq})}$  3 M, THF, reflux, 20 h; vi) 1)  $\text{NaOH}_{(\text{aq})}$  30 wt %, ethoxyethanol, reflux, 30 min, 2)  $\text{HCl}$  6 M; and vii) DIPC, DPTS,  $\text{CH}_2\text{Cl}_2$ , RT, 20 h.

## Results and Discussion

### Modular synthesis of fluorescent azo derivatives and monofunctional model systems:

The bifunctional and monofunctional model compounds are depicted in Schemes 1 and 2. All of them involve a bis(4'-tert-butylbiphenyl-4-yl)aminophenyl unit, the steric crowding and structural twist of which impairs intermolecular aggregation.<sup>[40,41]</sup> The electron-donating phenylamino core, connected to an electron-withdrawing group (azo or nitro) in the *para* position, imparts strong charge transfer. Both fluorophores **6** (**fluo1**) and **8** (**fluo2**) were obtained following a Hartwig-Buchwald cross-coupling between the secondary aromatic amine **5** and the arylbromides **2** and **4** in the presence of  $\text{Cs}_2\text{CO}_3$  as a mild base to avoid hydrolysis of the ester introduced as a protecting group of the hydroxyl and carboxyl functions (Scheme 1). After depro-



Scheme 2. Synthesis of the photochromic azo and bifunctional compounds. i) 4-Nitrosobenzoic acid,  $\text{AcOH}/\text{DMSO}$ , RT, 48 h; ii) DIPC, DPTS,  $\text{CH}_2\text{Cl}_2$ , RT, 12 h; and iii)  $\text{SOCl}_2$ ,  $\text{MeOH}$ , 40°C, 2 h.

tection in alkaline solution, compounds **7** and **9** were involved in a mild esterification reaction catalyzed by diisopropylcarbodiimide (DIPC)/4-(dimethylamino)pyridinium *p*-toluenesulfonate (DPTS) as a coupling agent, thus leading to the model compound **11** (**fluo2-SP**) and the bifunctional azo compound **15** (**azo-fluo1**), respectively (Scheme 2). A second modular approach allowed us to generate the azo carboxylic intermediate **13** from reaction between the primary aromatic amine **12** and 4-nitrosobenzoic acid (Scheme 2). Subsequent esterification of **13** with the diphenol spacer **10**, by following the same protocol as that previously described, generated the model azo compound **16** (**azo-SP**). Further esterification of **azo-SP** was performed with the diarylamino benzoic acid **9** to eventually conduct to the second bifunctional molecule **17** (**azo-SP-fluo2**) in which both the azo and fluorescent units were attached through a 10 Å-long spacer.

Choice of the Diels–Alder adduct **10** as a linker, synthesized from 2,6-anthraflavic acid,<sup>[42]</sup> was motivated by its rigid and nonconjugated backbone along with the existing reactive hydroxyl functions. It was systematically reacted in a twofold excess amount with respect to the carboxylic acids **9** and **13** to minimize diester formation. The monoester products **11** and **16** were easily isolated as pure compounds by column chromatography. Finally, compared to a synthetic route toward **azo-SP-fluo2**, which could have involved **fluo2-SP** and **13**, the adopted synthetic strategy, based on **azo-SP** and **9**, allowed us to easily discard by chromatography purification any trace of unreacted fluorophore that could blur the time-resolved and steady-state emission analyses.

**Steady-state UV/Vis spectroscopy:** All the photophysical measurements were performed on solutions in toluene in which both the fluorescent and azo compounds exhibit high solubility. The absorption spectra of the monofunctional compounds **fluo1**, **fluo2**, **fluo2-SP**, **azoE**, and **azo-SP** display two bands (Figure 1). The first band is invariably located in the UV range around 320–330 nm and could be ascribed to biphenylamino core-centered transitions from time-dependent TDDFT calculations (vide infra) and prior comparative studies. For the fluorophores **fluo1**, **fluo2**, and **fluo2-SP** (Table 1), the second band ( $\lambda_{\max}$  around 410 nm) could be attributed to a  $\pi$ – $\pi^*$  transition with strong charge-transfer CT character from the triphenylamino core to the nitro group. For the azo compounds **azoE** and **azo-SP** (Table 2), a  $\pi$ – $\pi^*$  (CT) band is observed with  $\lambda_{\max}$  around 470 nm. Similar spectral features were also noticed for the bifunctional compounds **azo-fluo1** and **azo-SP-fluo2** except that both CT bands overlapped and led to a broad absorption in the visible region. The maximum absorption wavelength of the fluorescent

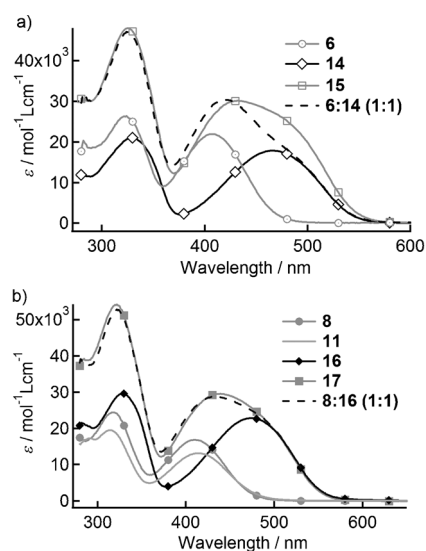


Figure 1. UV/Vis absorption spectra of solutions of a) the monofunctional model fluorophores **fluo1**, **fluo2**, and **fluo2-SP**. b) the monofunctional azo models **azoE** and **azo-SP**, the bifunctional compounds **azo-fluo1** and **azo-SP-fluo2**, the stoichiometric mixture of azo and fluorophore models **azoE:fluo1** and **azo-SP:fluo2** in toluene.

Table 1. Steady-state absorption and emission maxima, fluorescence quantum yields, and fluorescence decay times of solutions of the model and bifunctional fluorophores in toluene.

Compound	$\lambda_{\max}(\text{abs})$ [nm]	$\lambda_{\max}(\text{em})$ [nm]	$\Phi_f^{[a]}$	$\tau_f$ [ns] <sup>[b]</sup> (fraction $f_i$ ) <sup>[c]</sup>
<b>fluo1</b>	408, 324	587	0.085	1.9
<b>fluo2</b>	411, 318	614	0.035	0.91
<b>fluo2-SP</b>	416, 318	625	0.021	0.6 (90%), 0.2 (10%)
<b>azo-fluo1</b>	431, 325	590	$< 10^{-4}$	0.6 (20%), 0.1 (80%)
<b>azo-SP-fluo2</b>	439, 320	620	0.022	0.5 (80%), 0.2 (20%)

[a] Coumarine 540A in ethanol used as a fluorescence standard,  $\Phi_f = 0.38$ .<sup>[65]</sup> [b] Excitation was performed at 410 nm and emission was collected at 600 nm. [c] Fluorescence decays were modeled by a monoexponential or biexponential law  $I_f(t) = a_1 \exp(-t/\tau_1) + a_2 \exp(-t/\tau_2)$  in which the normalized fraction  $f_i$  is defined by  $f_i = \frac{a_i \tau_i}{\sum_j a_j \tau_j}$ .

units almost matches the minimum absorption wavelength of the azo units (Figure 1), which allows for quite selective irradiation of both units. Insignificant electronic interactions in the ground state between the bridged fluorescent and azo

Table 2. UV/Vis absorption maxima and photochromic properties of solutions of the monofunctional and bifunctional azo compounds in toluene.

Compound	$\lambda_{\max}(\text{abs})$ [nm]	$k^{[a]}$ [ $10^{-5} \text{ s}^{-1}$ ]	$\Phi_{EZ}^{[b]}$	$\Phi_{ZE}^{[b]}$	$\rho$ [%] <sup>[c,d]</sup>	$\epsilon_Z$ [ $\text{mol}^{-1} \text{ L cm}^{-1}$ ] <sup>[d]</sup> ( $\lambda_{\text{obs}}$ [nm])
<b>azoE</b>	465, 330	8	$0.35 \pm 0.02$	$0.7 \pm 0.1$	$65 \pm 3$	4500–5000 (467)
<b>azo-SP</b>	473, 328	9.8	$0.20 \pm 0.02$	$0.6 \pm 0.1$	$60 \pm 2$	5000–5500 (473)
<b>azo-fluo1</b>	431, 325	6.3	$0.15 \pm 0.01$	$0.6 \pm 0.1$	$60 \pm 2$	7000–7500 (470)
<b>azo-SP-fluo2</b>	439, 320	10.6	$0.21 \pm 0.01$	$0.6 \pm 0.1$	$58 \pm 2$	8000–9000 (470)

[a] Rate constant for the thermal *Z*–*E* isomerization obtained by a monoexponential fit of the temporal absorbance evolution of a solution previously prepared to a photostationary state by irradiation at 488 nm. [b] Quantum yields for photoisomerization. [c]  $\rho = [Z]/[E]_0$  with  $[E]_0$  the initial concentration of the azo solution before irradiation and  $[Z]$  the concentration of the *Z* photoisomers generated at the photostationary state. [d] Computed values using the least-squares method described in the Supporting Information.

units in **azo-SP-fluo2** are apparent from the superimposition of its experimental absorption spectrum with the calculated spectrum of a 1:1 mixture of model compounds **azo-SP** and **fluo2**. For the shorter bifunctional compound **azo-fluo1**, the match between its absorption spectrum and the calculated spectrum of a 1:1 mixture of fluorophore **fluo1** and azo compound **azoE** is not perfect. This suggests intramolecular interactions in the ground state and possible  $\pi$  stacking between the two photoactive units, permitted by the folding of the flexible alkyl chain.

Whereas the monofunctional azo compounds in fluid toluene solution are expectedly nonfluorescent, the model fluorophores **fluo1**, **fluo2**, and **fluo2-SP** were found to emit in the orange region at 587, 614, and 625 nm, respectively, far away from the azo absorption band (Table 1). The large Stokes shifts of  $7500\text{ cm}^{-1}$  for **fluo1** and  $8150\text{ cm}^{-1}$  for **fluo2** and **fluo2-SP** are attributed to an extensive geometry distortion in the excited state, as detailed below (see the transient absorption spectroscopy). The fluorescence quantum yields ( $\Phi_f$ ) were found to be 0.085, 0.035, and 0.021, respectively. The value of  $\Phi_f$  dramatically dropped to  $<10^{-4}$  for the bifunctional compound **azo-fluo1**, which displays barely detectable emission centered at 590 nm. By contrast, compound **azo-SP-fluo2** exhibits a clear fluorescence signal around 620 nm characterized by almost the same value of quantum yield  $\Phi_f=0.022$  as that for **fluo2-SP** (Figure 2a). Excitation spectra recorded at 620 nm clearly showed that emission exclusively originates from the fluorescent unit (Figure 2b). The dramatic 100-fold decrease of  $\Phi_f$  when going from **fluo1** to **azo-fluo1** is to be attributed to the close vicinity of the azo unit and the fluorescent moiety in **azo-fluo1**, whereas the rigid linker present in **azo-SP-fluo2**

allows for efficient electronic isolation of both chromophores.

**Frontier molecular orbitals (MOs) and electronic transitions:** Ab initio density functional theory (DFT) calculations were performed to evaluate the degree of electronic interactions in the ground state between the azo and fluorescent units and to help identify the absorption bands, especially for the bifunctional systems. The use of the B3LYP functional along with the 6-31G(d) basis set provided a good correlation between the energy transitions and the experimental spectroscopic features reported above. The charge-transfer transitions responsible for the investigated photoactivity (photochromism and fluorescence) occur in the visible region. Therefore the 4-*tert*-butylbiphenyl substituents, which participate only in UV transitions,<sup>[41]</sup> were simplified to tolyl groups to reduce computational costs (the corresponding compounds are denoted by s, e.g., **sazoE**; Figure S2 in the Supporting Information). For all azo compounds, computations were performed only on the *E* isomers, which are the exclusive species that exist at room temperature before irradiation.

For the monofunctional azo compounds **sazoE** and **sazo-SP**, the pictorial description of the frontier orbitals shows strong localization of the electronic density on the triphenylamino core ( $\pi$ -type HOMO) or on the azo N=N double bond (Table S1 in the Supporting Information). The latter group supports a lower-energy n-type bonding MO (HOMO-1 for **sazoE** and HOMO-2 for **sazo-SP**) as well as a  $\pi^*$  antibonding MO (LUMO). TDDFT calculations predict two electronic transitions of n- $\pi^*$  and  $\pi$ - $\pi^*$  character in the visible region, which correspond to the HOMO-1 (HOMO-2)→LUMO and HOMO→LUMO charge transfers for **sazoE** (**sazo-SP**), respectively. The absorption wavelengths are estimated very close at 501/503 nm and 479/484 nm, respectively, for **sazoE/sazo-SP** (Table S2 in the Supporting Information). The oscillator strength  $f$  of the symmetry-forbidden n- $\pi^*$  transition is found to be 50 to 100 times lower than that of the  $\pi$ - $\pi^*$  transition, as commonly reported for azo derivatives. An additional highly permitted third transition ( $f=0.549$ ) is evidenced in the UV region at 328 nm. It features an exclusively azo-located  $\pi$ - $\pi^*$  transition, as encountered for symmetric azo compounds.

It is worth mentioning the indirect correspondence of the transition energy ordering with regards to the MO energy levels of the azo derivatives due to electronic reorganization and configuration interactions in the excited states. For compound **sazo-SP**, a fourth transition (HOMO-1→LUMO) that involves charge transfer from the rigid bridge could be identified at 454 nm. Due to its very low oscillator strength ( $f=3\times 10^{-3}$ ), the corresponding excited state is formed in a minor amount upon excitation in the visible region, and its electronic influence onto the photochromic and fluorescent properties of the compounds is considered negligible.

The fluorescent compounds **sfluo1**, **sfluo2**, and **sfluo2-SP** invariably present HOMOs localized on the triphenylamino core, whereas the LUMOs are spread on the nitrophenyl

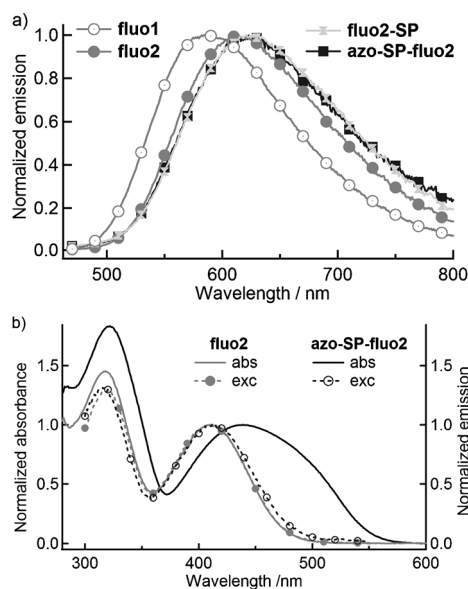


Figure 2. a) Normalized emission spectra of solutions of the model fluorophores **fluo1**, **fluo2**, **fluo2-SP**, and bifunctional **azo-SP-fluo2** compounds in toluene ( $\lambda_{\text{exc}}=420\text{ nm}$ ). b) Normalized absorption and excitation spectra ( $\lambda_{\text{em}}=620\text{ nm}$ ) of solutions of compounds **fluo2** and **azo-SP-fluo2** in toluene.

moiety (Table S1 in the Supporting Information). It is worth noting that the ester or benzylic groups do not participate in the LUMO in accord with their *meta* position, electronically decoupled from the 4-aminonitrophenyl unit. Therefore the HOMO→LUMO transitions are not significantly affected and occurred around 403–406 nm except for **fluo2-SP** in which the HOMO is on the Diels–Alder bridge (Table S2 in the Supporting Information). The *meta* substitution had indeed been deliberately chosen when devising the molecules, so that the amino–nitro charge transfer and the related emissive excited state remained little affected.

The combination of both chromophores in the bifunctional systems **sazo-fluo1** and **sazo-SP-fluo2** generates MO wavefunctions, the electronic density of which is again clearly located on each separate chromophore. As depicted above, the triphenylamino cores provide high-energy occupied orbitals. For both compounds, the HOMO is rather located on the azo side, whereas the HOMO–1 for **sazo-fluo1** (HOMO–2 for **sazo-SP-fluo2**) is on the fluorophore side (Figure 3). The bonding n-type MO localized on the azo N=N double bond is featured by the HOMO–2 (HOMO–3 for **sazo-SP-fluo2** since the HOMO–1 is spread again on the Diels–Alder bridge). Finally, the LUMO and LUMO+1 are also principally developed on the electron-withdrawing

groups, namely, the azo and nitrophenyl units, respectively. Eventually, three main transitions in the visible region are obtained from TDDFT: the n-type azo-based HOMO–2 (or HOMO–3)→LUMO at 502 nm, the  $\pi$ -type azo-based HOMO→LUMO at 483–484 nm, and finally the fluorophore-based HOMO–1 (HOMO–2)→LUMO+1 at 405–407 nm. Hence, the azo and fluorescent units are quite effectively electronically decoupled in the ground state regardless of the linker. Since both units appear to interact in **azo-fluo1** from its experimental absorption spectrum, through-space intramolecular interactions permitted by the alkyl chain folding should also be taken into account. This shows that simple calculations, although they provide a nice description of the electronic density and MO energies, encounter several limitations for complex systems in which various conformations are possible.

**Kinetics and quantum yields of photochromic reactions:** The *E*→*Z* photoisomerization for all azo compounds was investigated in toluene upon irradiation at 488 nm at which the azo units almost exclusively absorb (97% of the light absorbed by the azo unit against 3% by the fluorophore). The in situ dynamics of the *E*→*Z* photoreaction was followed by recording UV/Vis absorption spectra. All the solutions were

prepared in the dark before irradiation to avoid partial *E*→*Z* conversion induced by ambient light. During irradiation, the intensity of the visible band strongly decreased due to the isomerization of the *E* forms into their less-absorbing *Z* photoisomers. No shift of the maximum wavelength occurred for the monofunctional azo compounds **azoE** and **azo-SP**. By contrast, a hypsochromic shift was observed for the bifunctional compounds **azo-fluo1** and **azo-SP-fluo2**. It originated from the absorption contribution of the fluorophore units, which is stronger than that of the newly generated *Z* azo units. For all compounds, three isosbestic points could clearly be observed at 560, 410, and 355 nm, thus indicating the formation of a single photoisomer (Figure 4). The rate constants *k* of the thermal back isomerization were determined after the photostationary state (PSS) had been reached. The *E* azo band recovery at wavelengths at which the major spectral changes occur followed a first-

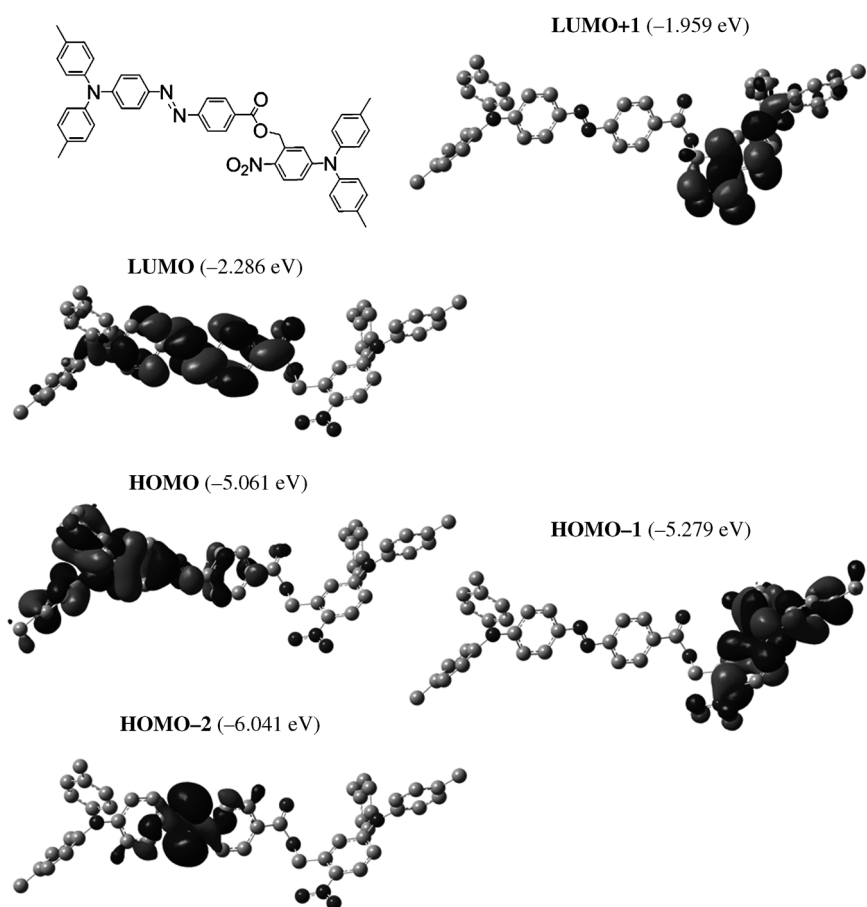


Figure 3. Pictorial description of the frontier orbitals for compound **sazo-fluo1** and the corresponding energies [eV] (DFT computations in the gas phase by using B3LYP/6-31G(d)).

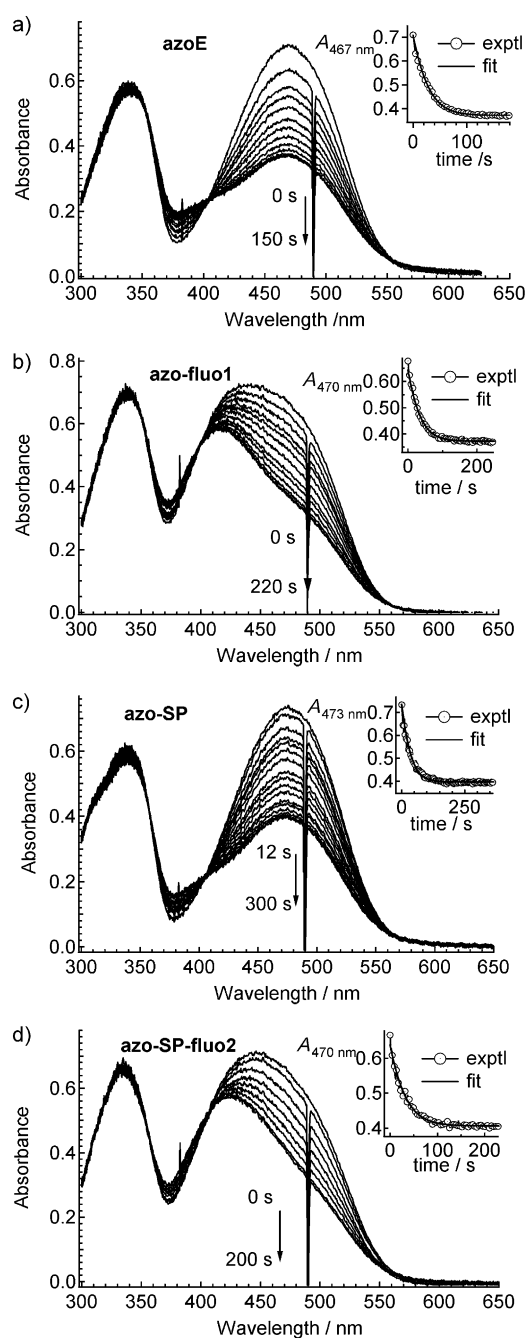


Figure 4. Time evolution of the absorption spectra of solutions of compounds a) **azoE**, b) **azo-fluo1**, c) **azo-SP**, and d) **azo-SP-fluo2** in toluene in the course of irradiation at 485 nm ( $30 \text{ mW cm}^{-2}$ ). Inset: experimental absorbance decay at the absorbance maximum wavelength and computed fit.

order kinetic law [Eq. (1)] in accord with the formation of single  $Z$  photoisomers.

$$[E]_t = [E]_0 + ([E]_{\text{PSS}} - [E]_0) \exp(-kt) \quad (1)$$

A slight acceleration of the  $Z \rightarrow E$  thermal back relaxation could be noted for the azo compounds that contained the Diels–Alder bridge since the rate constants  $k$  were around

$10 \times 10^{-5} \text{ s}^{-1}$  for **azo-SP** and **azo-SP-fluo2**, respectively, against  $6\text{--}8 \times 10^{-5} \text{ s}^{-1}$  for **azo-fluo1** and **azoE** (Table 2). The values are similar to those measured for analogous cyano-substituted aminoazo compounds since both the cyano and carboxylate groups exert comparable electron-withdrawing character. Clearly, the presence of bulky or fluorescent groups in compounds **azo-fluo1** and **azo-SP-fluo2** does not impede the photoisomerization reaction in fluid solutions.

This observation was confirmed through the photoconversion yield  $\rho = 1 - [E]_{\text{PSS}}/[E]_0$  and the quantum yields  $\Phi_{EZ}$  and  $\Phi_{ZE}$  of the photoreactions  $E \rightarrow Z$  and  $Z \rightarrow E$ , respectively. The latter two parameters were determined numerically from solving the time-dependent equation [Eq. (2)], which describes all the processes that take place during irradiation in which  $I_i$  features the photon flux absorbed by the species  $i$  at the molar concentration  $[i]$ :

$$d[E]/dt = -\Phi_{EZ}I_E + \Phi_{ZE}I_Z + k[Z] \quad (2)$$

If  $I_0$  designates the incident photon flux at the irradiation wavelength  $\lambda$ , Equation (2) can be written as follows [Eq. (3)]:

$$d[E]/dt = -\Phi_{EZ} \text{Abs}(E)I_0F + \Phi_{ZE} \text{Abs}(Z)I_0F + k[Z] \quad (3)$$

in which  $F = (1 - 10^{-\text{Abs}})/\text{Abs}$ , which is called the photokinetic factor (Abs corresponds to the total absorbance of the solution at the irradiation wavelength  $\lambda$ ;  $\text{Abs} = (\epsilon_E[E] + \epsilon_Z[Z])l$  in which  $\epsilon_i$  is the molar absorption coefficient of the species  $i$  and  $l$  the optical pathway of the solution).

Equation (3) can be unambiguously solved when the molar absorption coefficients  $\epsilon_E$  and  $\epsilon_Z$  of the  $E$  and  $Z$  forms, respectively, are known in addition to the value of  $k$  and the composition of the photostationary state. This is often encountered for P-type photochromes such as diarylethenes or fulgides, the open and closed isomers of which are both thermally stable and can be isolated. Azo compounds, referred to as T-type photochromes, give with few exceptions<sup>[43]</sup> mixtures of  $E$  and  $Z$  forms upon irradiation. We thus scanned a range of possible values for  $\epsilon_Z$  that provided the best fits with the boundary conditions  $\rho_{\min} \leq \rho \leq 1$  in which  $\rho_{\min}$  refers to the minimum conversion yield obtained from assuming nonabsorbing  $Z$  species at the wavelength of  $E$  maximum absorbance (in our case,  $\rho_{\min} \approx 0.5$  for all the azo compounds). The larger  $\epsilon_Z$  values screened for the bifunctional compounds **azo-fluo1** and **azo-SP-fluo2** stem from the contribution of the fluorophore units at the  $Z$  absorption maxima (467–470 nm). They were calculated to be  $2300 \text{ cm}^{-1} \text{ mol}^{-1} \text{ L}$  and  $2800 \text{ cm}^{-1} \text{ mol}^{-1} \text{ L}$  from the molar absorption coefficients of **6** and **8**, respectively (Figure 5; see the Supporting Information). The estimated values of  $\rho$ ,  $\Phi_{EZ}$ ,  $\Phi_{ZE}$ , and  $\epsilon_Z$  are reported in Table 2 at the maximum variation wavelength. In accord with the few data available in the literature, the photoinduced back reaction  $Z \rightarrow E$  was systematically found to be more efficient than the  $E \rightarrow Z$  photoisomerization. The  $\Phi_{ZE}$  value was nearly constant for all compounds ( $\Phi_{ZE} = 0.7 \pm 0.1$  for **azoE**,  $0.6 \pm 0.1$  for **azo-**

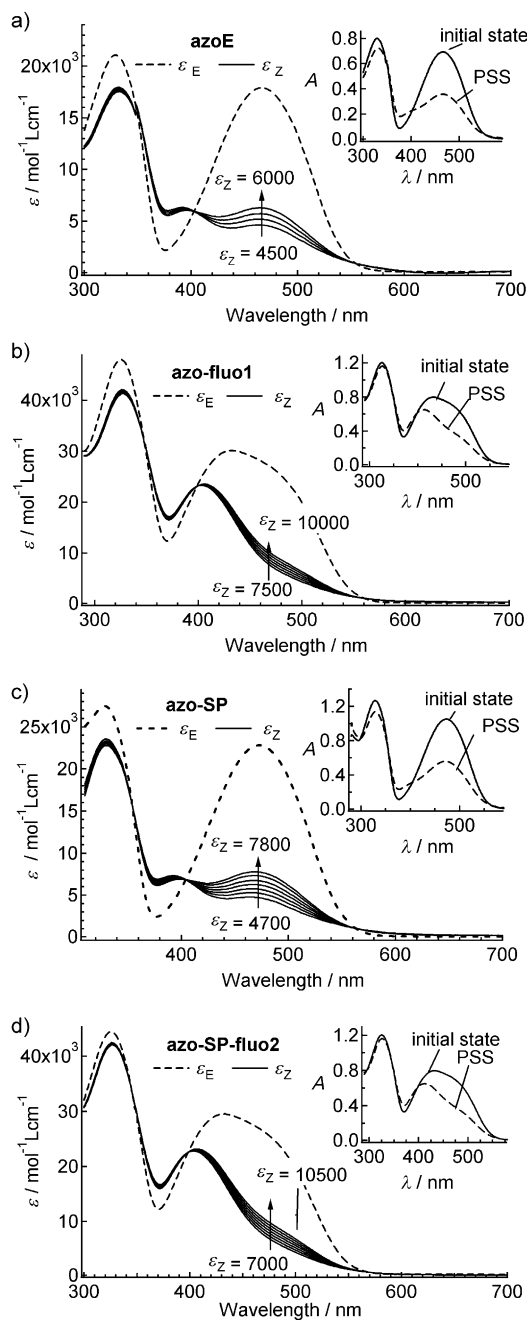


Figure 5. Modeling of the absorption spectra of the Z species after irradiation of solutions of the monofunctional a) **azoE**, c) **azo-SP** and bifunctional b) **azo-fluo1**, d) **azo-SP-fluo2** compounds in toluene. The different spectra in bold lines correspond to the computed absorption spectra of the Z isomer as a function of the indicated molar absorption coefficients of the Z isomers. Inset for each compound: absorption spectra before irradiation at 485 nm and at the photostationary state (PSS).

**fluo1** and **azo-SP-fluo2**; Table 2). These values correlate well with those reported for two push-pull azo derivatives, Disperse Red 1 (DR1;  $\Phi_{ZE} = 0.70$ ) and 4-(dimethylamino)-4'-nitroazobenzene (DNAB;  $\Phi_{ZE} = 0.74$ ), which nicely validates our calculations.<sup>[44–47]</sup> It is worth mentioning that the back-reaction quantum yield for the symmetric azobenzene has similarly been calculated at 0.4–0.75. This tends to show

that the  $Z \rightarrow E$  process is little influenced by the structure of the azo units, unlike the thermal back relaxation and the photoinduced  $E \rightarrow Z$  photoisomerization. The reaction quantum yield  $\Phi_{EZ}$  was indeed found at  $0.35 \pm 0.02$  for the model azoester compound **azoE**, and decreased to  $0.15 \pm 0.01$  for **azo-fluo1**,  $0.20 \pm 0.01$  for **azo-SP**, and  $0.21 \pm 0.01$  for **azo-SP-fluo2**. The decrease in  $\Phi_{EZ}$  between the azoester **azoE** and the other three compounds is likely to be due to the attachment of a bulky group at the ester side. This latter may induce larger geometry reorganization of the reactive excited state, thereby leading to energy loss at the expense of photoisomerization. The similar photoreactivities of the monofunctional azo adduct **azo-SP** and bifunctional compound **azo-SP-fluo2** show that the fluorophore unit influences the azo photoisomerization little. To shed light on the origin of the fluorescence quenching in the bifunctional compound **azo-fluo1** while the azo photoreaction was not impeded, we carried out further time-resolved fluorescence and femtosecond transient absorption studies.

**Time-resolved fluorescence decays and singlet excited-state lifetimes:** The fluorescence decays were measured at the emission maximum on solutions in toluene upon excitation at 410 nm, at which the fluorophore units mostly absorb. They were found to be monoexponential for both monofunctional fluorophores **fluo1** and **fluo2**, thus providing fluorescence lifetimes ( $\tau_f$ ) of 1.9 and 0.91 ns, respectively (Table 1). By contrast, compound **fluo2-SP** shows a biexponential decay with a major and a minor lifetime component of 0.6 ns (80%) and 0.2 ns (20%), respectively (Figure S2 in the Supporting Information). The decrease in  $\tau_f$  from **fluo2** to **fluo2-SP** mostly relates to the increasing contribution of the radiationless processes. When considering the major lifetime decay, the corresponding rate constants  $k_{nr}$  increased from  $1.0 \times 10^9 \text{ s}^{-1}$  for **fluo2** to  $1.6 \times 10^9 \text{ s}^{-1}$  for **fluo2-SP**, whereas the fluorescence rate constant  $k_f$  is only slightly affected (**fluo2**:  $3.9 \times 10^9 \text{ s}^{-1}$ , **fluo2-SP**:  $3.5 \times 10^9 \text{ s}^{-1}$ ). This again validates our design strategy that consists of anchoring linkers in the *meta* position of the 4-nitrophenylamine of the fluorophore, which did not electronically interfere with the radiative nitrophenylamine intramolecular charge transfer (ICT) excited state.

When the azo and fluorophore units are connected with a short spacer as in **azo-fluo1**, the fluorescence decay time dramatically decreases from 1.9 to 0.6 ns (20%) and 0.1 ns (80%) (Figure S2 in the Supporting Information). The fluorescence lifetimes of compound **azo-SP-fluo2**, with the Diels–Alder bridge inserted between the azo and the fluorescent units, were found to be 0.5 ns (80%) and 0.2 ns (20%), very similar to those measured for **fluo2-SP**. The striking contrast between the lifetimes of **azo-fluo1** and **azo-SP-fluo2** is obviously related to the introduction of the spacer between the fluorescent unit and the energy-scavenging azo group. Doubts could be cast on the origin of fluorescence in **azo-SP-fluo2**. However, traces of unreacted fluorophore are unambiguously to be ruled out on account of the synthetic pathway and purification strategy adopted

(Scheme 2). Moreover, both the fluorescence quantum yield and lifetime of **azo-SP-fluo2** decrease by at least one order of magnitude relative to those of **azo-fluo1**. Finally, no degradation was observed from the absorption spectra before and after irradiation. To explain this strong difference in fluorescence decays between the bifunctional compounds **azo-fluo1** and **azo-SP-fluo2**, we have estimated the Förster energy-transfer rate constant  $k_{\text{et}}$  from the spectral overlap factor and interchromophore distances (see the Supporting Information). The rate constant  $k_{\text{et}}$  was found to be  $4.4 \times 10^{12} \text{ s}^{-1}$  for **azo-fluo1**, whereas  $k_{\text{et}} = 8.2 \times 10^8 \text{ s}^{-1}$  for **azo-SP-fluo2**, almost four orders of magnitude smaller. Aside from its intrinsic relaxation pathways (internal conversion and intersystem crossing), the excited state of fluorophore **azo-fluo1** predominantly deactivates through energy transfer to the azo unit, hence fluorescence is efficiently quenched. Conversely, in compound **azo-SP-fluo2**, deactivation by fluorescence ( $k_{\text{f}} = 3.5 \times 10^9 \text{ s}^{-1}$ ) can efficiently compete with energy transfer. To assess further the role of the spacer, which appears to be crucial in the photophysics of the bifunctional compounds, femtosecond transient absorption spectroscopy studies were carried out.

**Femtosecond transient absorption spectroscopy of the monofunctional azo compounds azoE and azo-SP:** Pump-probe absorption spectra were recorded in toluene in the 350–800 nm range following excitation at 400 or 500 nm to address the fluorophore or the azo moiety, respectively. We first investigated the monofunctional compounds before analyzing the bifunctional ones. The solutions of all the monofunctional azo and bifunctional compounds were first prepared in a photostationary state by means of a 488 nm continuous irradiation, which was maintained throughout the pump-probe experiments. This enables data accumulation with no need to refresh the solution during each pump-probe experiment as absorbance changes due to  $E \rightarrow Z$  photoisomerization are avoided. The previous time-resolved fluorescence measurements, performed at 420 nm, had indeed revealed a 10% hypochromic change in the azo maximum absorption band, which could blur spectral interpretations otherwise.

The transient absorption (TA) spectra of the monofunctional azo compounds **azoE** and **azo-SP** exhibit similar spectral features and two-step ultra-short dynamics (Figure 6). No matter which excitation was employed (400 or 500 nm), the transient dynamics were found to be the same. Within 3 ps after excitation, a negative band that corresponded to the ground-state bleaching formed at 465 nm for **azoE** and **azo-SP**. A positive absorption band simultaneously rose at 550 and 555 nm for **azoE** and **azo-SP**, respectively. Both transients van-

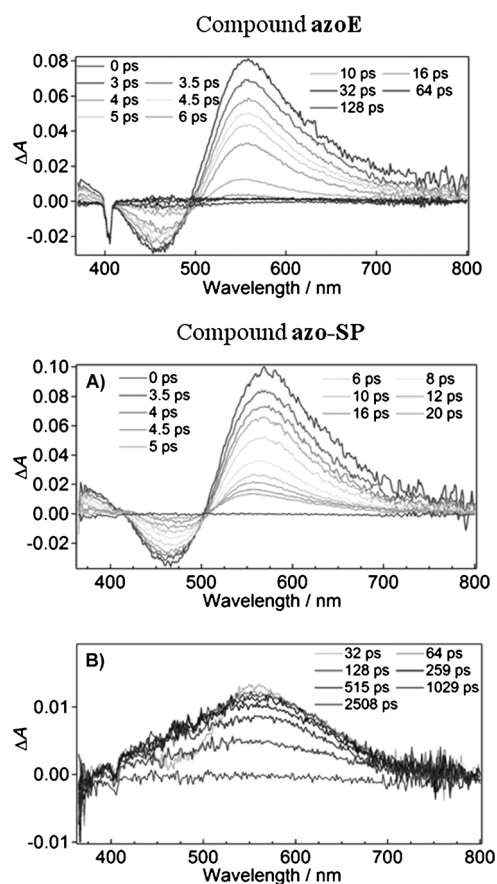


Figure 6. Transient absorption spectra of the model azo compounds **azoE** (top) and **azo-SP** (bottom) in toluene at different time delays after excitation at 400 nm. For clarity, the spectral evolution is separated in two time domains A) 0–20 ps and B) 32–2500 ps for compound **azo-SP**. The pump-probe time delays are displayed.

ished after 32 ps. Global fit analyses performed at the evolution maximum wavelengths revealed a two-step relaxation dynamics characterized by the time constants  $\tau_1 = 1.7$  ps and  $\tau_2 = 4.4$  ps for **azoE**, and  $\tau_1 = 1.2$  ps and  $\tau_1 = 4.5$  ps for **azo-SP** (Table 3; Figures S3 and S4 in the Supporting Information). These values are in the same range as those reported in the literature for push-pull molecules like DR1 (0.9 and 4.7 ps)<sup>[48]</sup> or 4-nitro-4'-dimethylaminoazobenzene (0.8 ps and

Table 3. Main time constants  $\tau_i$  averaged over kinetic analyses performed at various wavelengths related to the positions of the ground-state bleaching (GSB), transient absorption (TA), and stimulated emission (SE) bands.

Compound	$\lambda_{\text{exc}}$ [nm]	Transient decay time constant [ps]				Fluorescence lifetime [ps]
		$\tau_1$	$\tau_2$	$\tau_3$	$\tau_4$	
<b>fluo1</b>	400	1.2	22	1900		1900
<b>fluo2</b>	400	1.0	9.8	1000		910
<b>fluo2-SP</b>	400	0.7	25	200, 800	4500	200 (10%), 600 (90%)
<b>azoE</b>	500	1.7	4.4			–
<b>azo-SP</b>	500	1.2	4.5		> 2000	–
<b>azo-fluo1</b>	500	1.3	6			–
<b>azo-SP-fluo2</b>	400	9	15	100		100 (80%), 600 (20%)
	500	1.2	6.5			–
<b>azo-SP-fluo2</b>	400	1.2	6, 12	170, 600		200 (20%), 500 (80%)

around 5 ps).<sup>[49]</sup> The shorter component was attributed to the exploration by the  $S_1(n-\pi^*)$  excited state of the potential energy surface until reaching the conical intersection and undergoing photoisomerization.<sup>[36,48,50,51]</sup> The longer component corresponds to further vibrational cooling of the hot ground state  $S_0$  formed after photoisomerization. Our experiments did not allow us to observe the subpicosecond conversion of the  $S_2(\pi-\pi^*)$  excited state, formed right after pumping, toward the  $S_1(n-\pi^*)$ . This ultrafast conversion was actually reported to operate in fewer than 0.2 ps for DR1 and 4-aminoazobenzene.<sup>[46]</sup> Given the strongly allowed  $\pi-\pi^*$  transition for compound **azoE**, we can reasonably assume that the ground state is mainly depopulated after excitation due to  $S_2(\pi-\pi^*)$  population. Since no stimulated fluorescence could be observed, we assume that the excited state  $S_2(\pi-\pi^*)$  relaxes down to the  $S_1(n-\pi^*)$ , the radiative conversion of which to the ground state is prohibited by a weak oscillator strength (at least ten times as weak as that of  $S_2 \rightarrow S_0$  as shown through TD-DFT computations).

A broad absorption signal that spanned from 400 to 800 nm and centered at 550 nm was observed for **azo-SP** (Figure 6) and decayed in more than 2 ns. This feature is apparently related to the presence of the Diels–Alder adduct. Product degradation is not the cause of this signal, since the solution absorption spectrum is the same before and after irradiation. Moreover, nanosecond transient absorption spectroscopy (10 Hz frequency, Nd:YAG laser, 10 ns full width at half-maximum (fwhm), 355 nm excitation) does not show transient absorption at longer times. We suspect that the transient may be related to an excited state that involves the very weakly permitted charge-transfer transition from the Diels–Alder bridge to the LUMO that we estimate around 440–450 nm by theoretical computations (Table S2 in the Supporting Information).

**Femtosecond transient absorption spectroscopy of the monofunctional fluorophores fluo1, fluo2, and fluo2-SP:** The TA spectra of the monofunctional fluorophores **fluo1**, **fluo2**, and **fluo2-SP** show very similar evolution. Despite the structural simplicity of the fluorophores, the excited-state relaxation followed a quite complex three-step dynamics A=[0,4–6] ps, B=[4–6, 32–128] ps, and C=[32–128, >] ps. Each interval time limit depends on the examined compounds (Figure 7 and Figure S5 in the Supporting Information).

In the very first steps after excitation at 400 nm (period

A), a positive and intense absorption band rises at 454 nm. A negative signal simultaneously forms around 520 nm and undergoes progressive bathochromic shift to 570 nm. Finally a broad band, again positive, grows at longer wavelengths around 740 nm. Global fit analyses at each absorption maximum wavelength provide very similar time constants  $\tau_1$ , with values  $\tau_1(\mathbf{fluo1})=1.2$  ps,  $\tau_1(\mathbf{fluo2})=1.0$  ps, and  $\tau_1(\mathbf{fluo2-SP})=0.7$  ps, thereby revealing the dynamics of a single species (Table 3; Figures S6–S8 in the Supporting Information). Since excitation was performed in the lower-energy  $\pi-\pi^*$  CT band, the observed TA spectra are related to the formed charge-transfer excited state  $S_1$  that absorbs at 454 and 740 nm, with the negative signal at 520 nm being ascribed to a stimulated emission (SE) band. The slight shift observed for this latter band as well as the absorption band narrowing suggest that the dynamics observed over 4–6 ps are likely to result from solvent reorganization around the excited molecules and vibrational relaxation of the  $S_1$  excited states. Toluene solvation indeed operates with a 2.4 ps mean time constant.<sup>[52]</sup> In addition, different conformations due to the flexible units present in **fluo1**, **fluo2**, and **fluo2-SP** (triphenylamino core, biphenyl groups, nitro rotation, ester linker) exist in the ground state, which in turn leads to an inhomogeneous distribution of Franck–Condon (FC) excited states amenable to relaxation (Table 3).

In time interval B, which starts 4–6 ps after excitation, large spectral changes occur with the conservation of three clear isosbestic points near 430, 505, and 680 nm. The positive bands, initially centered at 460 and 740 nm, decrease with hypsochromic shifts of  $\Delta\lambda^{460}=-13/-19$  nm and  $\Delta\lambda^{740}=-60$  nm, respectively. In the same time, the negative SE

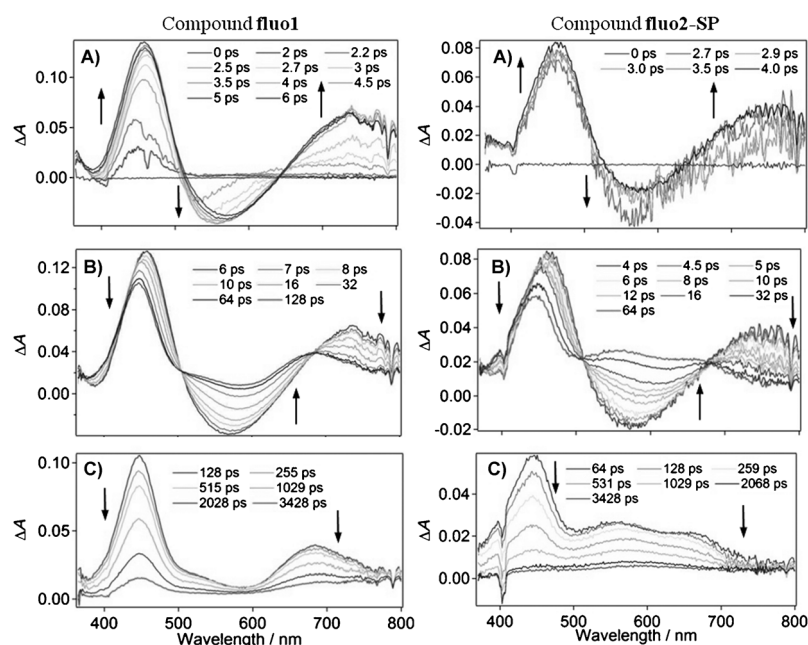


Figure 7. Transient absorption spectra of the model fluorophores **fluo1** (left) and **fluo2-SP** (right) in toluene at different time delays after excitation at 400 nm. For clarity, the spectral evolution is separated into three time domains A) 0–6 ps, B) 6–128 ps, and C) 128–3500 ps for compound **fluo1** and A) 0–4 ps, B) 4–64 ps, and C) 64–3500 ps for compound **fluo2-SP**. The pump–probe time delays are displayed.

band fades as it undergoes a bathochromic shift. The final wavelengths reached for the SE signals (585, 607, and 618 nm for **fluo1**, **fluo2**, and **fluo2-SP**, respectively) remarkably match those observed in the steady-state fluorescence spectra. Kinetic analyses of the 460 nm-centered TA band and the SE band reveal decay time constants  $\tau_2=22$  ps for **fluo1**,  $\tau_2=9.8$  ps for **fluo2**, and  $\tau_2=25$  ps for **fluo2-SP**. The large hypsochromic shifts of the TA bands, the presence of isosbestic points, and the stabilization of the SE band before fading suggest the evolution of the initial ICT state toward a new ICT' excited state, which follows strong geometrical distortions. Previous TA spectroscopy studies of nitroaromatic compounds have actually revealed large rotation of the nitro group with respect to the phenyl plane, which operates after the first ICT state had been formed.<sup>[53]</sup> This torsion is accompanied by a modest increase in the dipole moment and net stabilization of the excited state.<sup>[54]</sup> In our case, such a distortion has been confirmed by additional studies in more polar solvents like ethanol and acetonitrile, thereby causing an enhanced twist of the nitro group and radiationless relaxation of the ICT' state back to the ground state exclusively by means of internal conversion.<sup>[55]</sup>

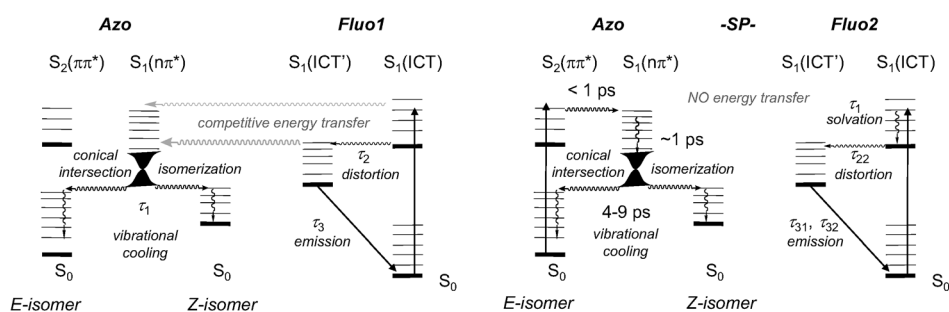
Finally, during the last time period C (starting at 128 ps after excitation for **fluo1**, 32 ps for **fluo2**, and 60 ps for **fluo2-SP**), the TA spectra decreased monoexponentially with a time constant  $\tau_3$  of 1.9 and 1.0 ns for compounds **fluo1** and **fluo2**, respectively. These decay times are in quite perfect agreement with the fluorescence decays measured by time-correlated single-photon counting (1.90 and 0.91 ns respectively). The TA decay of **fluo2-SP** followed a biexponential law with time constants  $\tau_{31}=0.2$  ns and  $\tau_{32}=0.8$  ns in nice accord with those measured by time-resolved fluorescence spectroscopy. To conclude this series of experiments, it has become clear that the large Stokes shifts observed for the 4-triphenylamino-4'-nitrophenyl compounds **fluo1**, **fluo2**, and **fluo2-SP** stem from the extensive geometrical reorganization and distortion of the ICT excited state  $S_1$  toward a novel radiative  $S_1(\text{ICT}')$  excited state, which operates in a few picoseconds in toluene solution (Scheme 3).

**Femtosecond transient absorption spectroscopy of the bifunctional azo compounds azo-fluo1 and azo-SP-fluo2:** Excitation was first performed at 500 nm to specifically address

the azo units. This allowed us to infer the spectral dynamics of the azo unit independently of the fluorophore unit. As reported for the monofunctional compounds, the TA spectra display the same negative signal at 470 nm, which characterizes the ground-state bleaching, and a strong positive signal centered at 570 nm, along with two isosbestic points at 420 and 500 nm (Figure S9 in the Supporting Information). Global kinetic analyses provide a two-step evolution almost identical to that reported for the monofunctional azo compounds **azoE** and **azo-SP**, namely, short  $\tau_1$  and longer  $\tau_2$  components that correspond to the decay of the  $S_1(n\pi^*)$  excited state, and the vibrational cooling of  $S_0$  formed after photoisomerization from  $S_1$ . The time constants were found to be  $\tau_1=1.3$  ps and  $\tau_2=6.0$  ps for **azo-fluo1**, and  $\tau_1=1.2$  ps and  $\tau_2=6.5$  ps for **azo-SP-fluo2** (Table 3). The slightly longer time constants  $\tau_2$  for the bifunctional compounds compared to those of the monofunctional azo systems (4.4 and 4.5 ps for **azoE** and **azo-SP**, respectively) is due to the larger size of the global azo backbone onto which the excitation is delocalized, thereby giving rise to a temporally extended lifetime decay.<sup>[56]</sup>

When excitation was performed at 400 nm, the transient absorption spectra were characterized by a mix of the spectral evolutions of the fluorophore and the azo units, which are both excited (Figure 8). A few picoseconds after excitation, the TA spectra of **azo-fluo1** and **azo-SP-fluo2** resemble each other with three positive TA bands centered at 460, 568, and 740 nm (time domain A). From the prior studies performed on the isolated azo and fluorescent units, the band at 460 nm results from the superimposition of the positive TA signal of the fluorescent unit and the negative ground-state bleaching (GSB) band of the azo unit. The band at 568 nm features the TA spectrum of the azo unit, in agreement with the maximum found at 570 nm when only the azo unit was excited by a 500 nm pulse. In this region, contrarily to the fluorophore models, no trace of the negative and intense SE band around 520 nm was detected due to the overlapping net transient absorption of the azo unit from 510 to 800 nm.<sup>[49]</sup> Finally, the last band at 740 nm mainly characterizes the fluorophore excited state. After the initial phase, the contribution to the spectra of the initially excited azo chromophore quickly disappears, in accordance with its short lifetime (Figure 8, graphs A).

The excited state of **azo-fluo1** mostly decays through energy transfer to the azo unit. The decay of the excited fluorophore can be monitored at the two positive bands around 458 nm and around 740 nm (Figure 9). The major component of 100 ps corresponds well with the main component of the fluorescence decay (0.1 ns). Faster processes with time constants  $\tau_1(\text{azo-fluo1})=9$  ps and  $\tau_2(\text{azo-fluo1})=15$  ps are also



Scheme 3. Scheme of the photophysical dynamics from TA global analyses for **azo-fluo1** and **azo-SP-fluo2** (this latter also features the photoisomerization dynamics of free azo units).

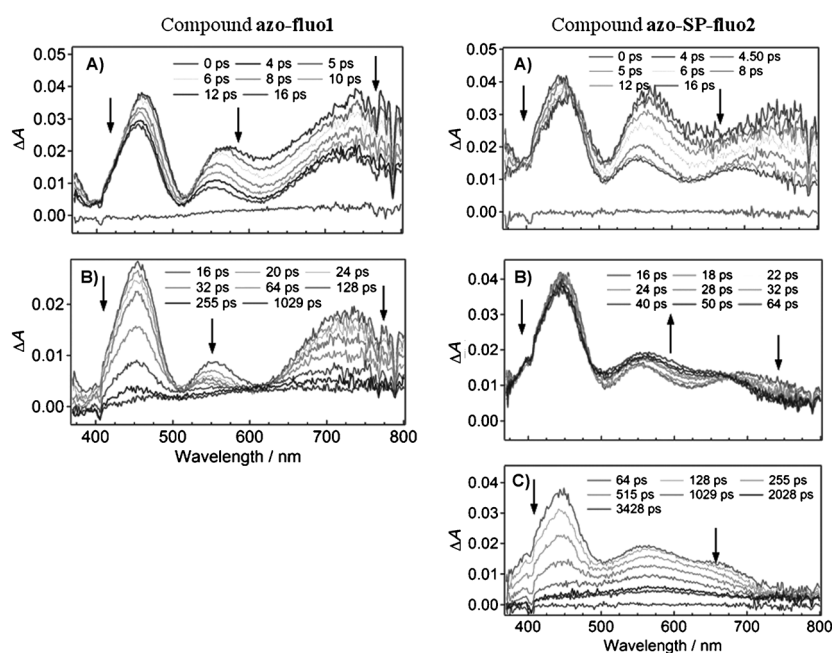


Figure 8. Transient absorption spectra of the bifunctional compounds **azo-fluo1** (left) and **azo-SP-fluo2** (right) in toluene at different time delays after excitation at 400 nm. For clarity, the spectral evolution is separated into three time domains A) 0–16 ps and B) 16–1030 ps for compound **azo-fluo1**, and A) 0–16 ps, B) 16–64 ps, and C) 64–3500 ps for compound **azo-SP-fluo2**. The pump–probe time delays are displayed.

observed and are likely to be related to structural reorganization in the excited state. Significantly smaller shifts could be noticed in the time domain B ( $>16$  ps) ( $\Delta\lambda^{460} = -7$  nm and  $\Delta\lambda^{740} = -15$  nm) relative to the fluorophore models **fluo1**, **fluo2**, and **fluo2-SP** ( $\Delta\lambda^{460} = -13/-19$  nm, and  $\Delta\lambda^{740} = -60$  nm). Stabilization of the newly formed ICT' excited state as encountered for the fluorophore models faces competing fast energy transfer to the azo unit. Interestingly, a weak positive absorption at 565 nm remains after the fast initial decay. This is a signature of the azo TA present in low concentration because it is generated more slowly than it decays.

The presence of an intense TA band around 730 nm could be confusing since it is also characteristic of a triphenylamine radical cation.<sup>[57,58]</sup> However, on thermodynamic grounds, charge transfer from the fluorophore to the azo unit could be discarded, especially in toluene, which is considered to be an apolar solvent unfavorable to intramolecular electron transfer. This band is present for all the fluorescent models from very early on. In addition, charge separation would cause significant spectral shifts,<sup>[59]</sup> which do not occur. The intense band thus features a strong intramolecular charge transfer excited state, which deactivates in 100 ps in a radiative manner.

The decay of **azo-SP-fluo2**, in which the energy transfer is strongly suppressed, resembles that of the model fluorophore **fluo2-SP**. After the initial fast decay at 560 nm (following direct excitation of the azo chromophore), a slow rise as well as significant blueshifts of the whole spectrum are observed (Figure 8 and Figure 10). This slower dynamics, which last up to 64 ps (Figure 8, time domain B on the

right), is characterized by the appearance of two isosbestic points at 485 and 675 nm, and recalls the progressive transformation of the ICT state of **fluo2-SP** into a more distorted excited state ICT'. Global analyses provided three decay time constants  $\tau_1(\text{azo-SP-fluo2}) = 1.2$  ps,  $\tau_{21}(\text{azo-SP-fluo2}) = 6$  ps, and  $\tau_{22}(\text{azo-SP-fluo2}) = 12$  ps. The shorter time  $\tau_1$  can not only feature the  $S_1$  ( $n-\pi^*$ ) relaxation of the azo unit, but also the solvation of the Franck–Condon excited state of the fluorophore unit as already described for **fluo2-SP**.  $\tau_{21}(\text{azo-SP-fluo2})$  characterizes the vibrational cooling of  $S_0(\text{azo})$  since its component prevails over [560–610] nm. The longer lifetime  $\tau_{22}(\text{azo-SP-fluo2})$  eventually pertains to the internal structural dynamics of the excited fluorophore. This can evolve

into a more distorted geometry ICT' state without being quenched by the energy transfer to the azo unit, which occurs in  $1/k_{\text{et}} = 0.2$  ps for **azo-fluo1** and is suppressed for **azo-SP-fluo2** (Scheme 3).

Finally, during interval C = [64 ps, >], the TA spectrum of **azo-SP-fluo2** homogeneously decreases following a biexponential decay characterized by  $\tau_{31} = 170$  ps and  $\tau_{32} = 600$  ps, close to the fluorescence lifetimes of **fluo2-SP** ( $\tau_f = 200$  and 500 ps) measured by time-correlated single-photon counting (TCSPC). We did not previously discuss the origin of the double fluorescence lifetime. It could be attributed to the existence of two conformations of the fluorophore unit with respect to the bridge due to possible free rotation around the C–O bond.

From the spectral evolution reported above, it appears that emission from the fluorophore unit operates from a distorted ICT' state, the stabilization of which competes with the energy transfer to the azo unit that is undergoing ultrafast photoisomerization (Scheme 3). Connecting both emissive and azo units by means of a long and rigid spacer suppresses not only efficiently Förster energy transfer, but can also modify the photomechanical properties, as evidenced below in bulk thin films subjected to illumination.

**Influence of the Diels–Alder adduct on the bulk molecular density:** All the previous studies have been performed in solution. When working with photoactive materials, the presence of bulky groups could impede the photochromic reaction due to steric constraints. It turns out that the longer bridge (Diels–Alder adduct) in **azo-SP** or **azo-SP-fluo2** did not inhibit the photoisomerization reaction but even favors

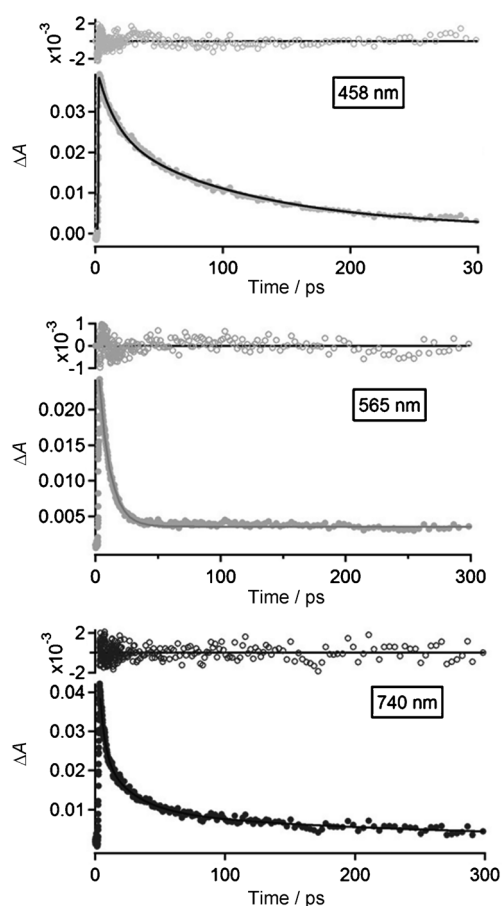


Figure 9. Experimental transient decay plots after excitation at 400 nm and best multiexponential fits using global analysis for compound **azo-fluo1**. Wavelengths at which modeling was performed are indicated on the graphs.

migration of the azo unit. Comparative holographic studies on isoabsorbing thin films ( $A \approx 1.1$ ), obtained from spin-coating concentrated solutions and exposed to interferential illumination,<sup>[60]</sup> showed that the azo migration, albeit slower for compound **azo-SP-fluo2** than for compound **azoE**, produces higher surface modulation for **azo-SP-fluo2** (Figure 11). Atomic force microscopy (AFM) measurements provided a peak-to-trough amplitude equal to 480 nm for **azo-SP-fluo2** against 240 nm for **azoE**. The thickness of films **azo-SP-fluo2** was found to be 570 nm, significantly larger than that of films of **azoE** (280 nm), thereby suggesting a less dense material. Similar comparisons between irradiated thin films of **azo-SP** and **azo-fluo1** showed that higher diffraction efficiency, which features deeper surface relief gratings, was again obtained for **azo-SP**, which contains the Diels–Alder unit. If migration seems to be ruled in the first minutes by the size of the group grafted to the azo unit (one can notice a slowdown from **azoE**, to **azo-fluo1/azo-SP**, and finally **azo-SP-fluo2**), the final photostationary state is rather governed by the free volume generated by the substituent itself. Such an assumption is confirmed by the values of the refractive index  $n$  measured by ellipsometry.

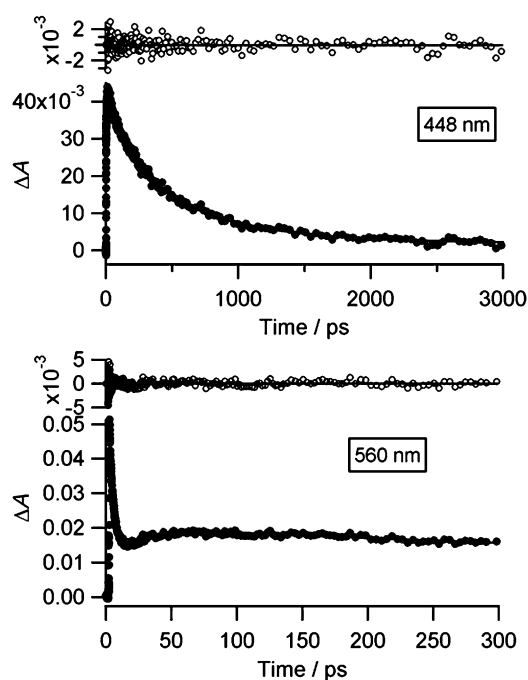


Figure 10. Experimental transient decay plots after excitation at 400 nm and best multiexponential fits using global analysis for compound **azo-SP-fluo2**. Wavelengths at which modeling was performed are indicated on the graphs.

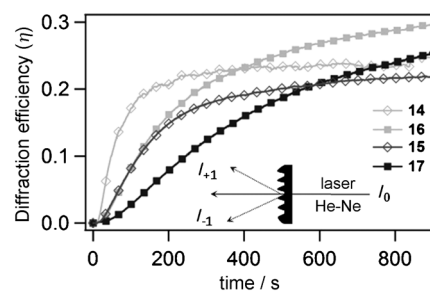


Figure 11. Temporal evolution efficiency  $\eta = (2I_{\pm}/I_0)$  of the first-order diffracted He–Ne laser beam ( $\lambda = 633$  nm) for azo thin films made of neat monofunctional **azoE** (14), **azo-SP** (16) or bifunctional **azo-fluo1** (15), **azo-SP-fluo2** (17) compounds, isoabsorbing at the azo absorption maximum wavelength ( $A \approx 1.1$ ) and subjected to a two-beam interferential illumination ( $\lambda = 488$  nm;  $160 \text{ mW cm}^{-2}$  per beam).

To a quite good approximation,  $n^2$  can be considered equal to the optical dielectric constant  $\epsilon_{\text{op}}$ , which is related to the electronic polarization and consequently to the material density. We found  $n$  at 600 nm smaller for **azo-SP-fluo2** ( $n = 1.722$ ) than for **azo-fluo1** ( $n = 1.750$ ).<sup>[61]</sup> This also holds true between the model fluorophores **fluo2** ( $n = 1.687$ ) and **fluo2-SP** ( $n = 1.642$ ), or the model azo compounds **azoE** ( $n = 1.770$ ) and **azo-SP** ( $n = 1.750$ ), **fluo2-SP**, and **azo-SP**, which both contain the Diels–Alder adduct. This spacer does not only provide enough electronic insulation to keep the emission almost unchanged but also favors larger free volume in the azo nanoenvironment, a prerequisite to molecular motion. The Diels–Alder adduct thus plays a role tanta-

mount to that of the triptyceny group, which has been largely used to create nanoporosity in thin films for enhanced diffusion of analytes, or facilitate film stretchability.<sup>[62]</sup> In this way, we have previously demonstrated for the first time that fluorescent gratings could be obtained that show a  $10^2$  emission contrast between the troughs and the crests on account of differential accumulation and migration of the azo compound **azo-SP-fluo2** and the simultaneous drag of the covalently linked fluorophore.

## Conclusion

In the search for photochromic azo molecular materials to form fluorescent patterns upon illumination, fluorescent units known to emit light in the solid state have been attached to azo moieties. Strong dependence of the fluorescence properties on the linker structure has been found, thereby prompting us to perform comparative measurements by using steady-state and time-resolved fluorescence, and femtosecond transient absorption spectroscopy in toluene solution, which mimics well the solid state. The photoisomerization quantum yields  $\Phi_{EZ}$  ( $\approx 0.15$ – $0.35$ ) and  $\Phi_{ZE}$  ( $\approx 0.6$ – $0.7$ ), as well as the photoconversion yields  $\rho$  ( $\approx 58$ – $65\%$ ) were found to be similar for the model and bifunctional molecules, thus proving the negligible electronic influence of the fluorophore on the photochromic behavior. Kinetic analyses of the femtosecond transient absorption spectra of the model and bifunctional systems reveal that the introduction of a triptyceny-like rigid and nonconjugated spacer between the azo and fluorescent units suppresses competitive energy transfer from the fluorophore to the azo moiety.

As such, both photoisomerization and fluorescence are conserved, which allows for the creation of fluorescent patterns in thin films exposed to interferential illumination. This structuration, which relies on multiple *E*–*Z* photoisomerization cycles of the azo units, is highly favored by the presence of the spacer. This creates additional free volume, compulsory for efficient azo bulk migration. These studies represent the first thorough examination of the photophysics of bifunctional compounds that contain structurally distinct push–pull fluorescent and azo units. The possibility to address both the emissive and photoisomerization properties at the same wavelength while recording redshifted emission opens exciting perspectives in the field of photoinduced locomotion and tracking at the single-molecule level.

## Experimental Section

**General:**  $^1\text{H}$  and  $^{13}\text{C}$ NMR spectra were recorded using a JEOL 400 MHz spectrometer and chemical shifts were reported in ppm relative to TMS or referenced to the residual solvent. High-resolution mass spectra were obtained by MALDI-TOF (Voyager DE-STR, Applied Biosystems). Melting points were measured by using a Kofler bench. Glass transition temperatures  $T_g$  were measured by using differential scanning calorimetry (Perkin–Elmer Pyris Diamond) in aluminum caps under nitrogen

flow at a scan rate of  $20^\circ\text{Cmin}^{-1}$  over the temperature range  $30$ – $250^\circ\text{C}$ . Spectroscopic grade toluene was used for spectroscopic measurements. All air-sensitive reactions were performed under argon using a vacuum line. The synthesis of compounds **1**–**8**,<sup>[63]</sup> **9**,<sup>[60]</sup> **10**,<sup>[42]</sup> **fluo2-SP**,<sup>[60]</sup> **12**,<sup>[40]</sup> **azo-SP**,<sup>[60]</sup> and **azo-SP-fluo2**<sup>[60]</sup> has been reported elsewhere. Spectroscopic grade solvents have systematically been used for steady-state and time-resolved photophysics.

**Synthesis of 4-[4-[bis(4'-tert-butylbiphenyl-4-yl)amino]phenylazo]benzoic acid (13):** A solution of Oxone (89.8 g, 146 mmol, 2 equiv) in water (450 mL) was added to a solution of 4-aminobenzoic acid (9.99 g, 72.8 mmol, 1 equiv) in dichloromethane (110 mL). The solution was stirred under argon at room temperature for 1 h. The precipitate was collected under vacuum, washed with water, and dried under vacuum over solid phosphorus pentoxide to yield quantitatively a crude yellow solid used with no further purification. 4-Nitrosobenzoic acid (570 mg, 3.82 mmol, 2 equiv) was dissolved in a mixture of DMSO/glacial acetic acid (1:1; 52 mL) under argon. Bis(4'-tert-butylbiphenyl-4-yl)-4-aminophenylamine **12** (1.0 g, 1.91 mmol, 1 equiv) was added portionwise, meanwhile the pale yellow solution turned deep brown-red. After stirring for 48 h at room temperature, a fine red product formed, which corresponded to the pure compound **13**. This was filtered off and washed well with water (1.2 mg, 95%).  $^1\text{H}$  NMR (400 MHz,  $\text{CDCl}_3$ , TMS):  $\delta$  = 8.22 (d,  $^3J(\text{H,H})$  = 8.7 Hz, 2H), 7.93 (d,  $^3J(\text{H,H})$  = 8.2 Hz, 2H), 7.88 (d,  $^3J(\text{H,H})$  = 8.7 Hz, 2H), 7.56 (d,  $^3J(\text{H,H})$  = 8.2 Hz, 4H), 7.55 (d,  $^3J(\text{H,H})$  = 8.7 Hz, 4H), 7.47 (d,  $^3J(\text{H,H})$  = 8.2 Hz, 4H), 7.27 (d,  $^3J(\text{H,H})$  = 8.7 Hz, 4H), 7.21 (d,  $^3J(\text{H,H})$  = 8.7 Hz, 2H), 1.37 ppm (s, 18H; *-t*Bu); HRMS (MALDI-TOF): *m/z* calcd for  $\text{C}_{45}\text{H}_{43}\text{N}_3\text{O}_2$  [ $M^+$ ]: 657.3355; found: 657.33498.

**Synthesis of methyl 4-[4-[bis(4'-tert-butylbiphenyl-4-yl)amino]phenylazo]benzoate (14):**  $\text{SOCl}_2$  (0.2 mL, 2.74 mmol, 6 equiv) was added to a solution of **13** (300 mg, 0.46 mmol, 1 equiv) in anhydrous dichloromethane (10 mL) under argon. The reaction mixture was heated to reflux for 2 h. After cooling to room temperature, the residual  $\text{SOCl}_2$  was evaporated and the resulting acid chloride was quenched with an excess amount of anhydrous methanol (5 mL). The solution was stirred at  $40^\circ\text{C}$  for a further 2 h and evaporated to dryness. After dissolution in dichloromethane, the solution was successively washed with a saturated solution of sodium hydrogen carbonate and water. The extracted organic layer was dried over anhydrous sodium sulfate. Concentration under vacuum followed by silica gel column chromatography using a 1:1 dichloromethane/petroleum ether mixture as an eluent afforded **14** (**azoE**) as an orange-red glassy solid (145 mg, 47%);  $T_g$  =  $68^\circ\text{C}$ .  $^1\text{H}$  NMR (400 MHz,  $\text{CDCl}_3$ , TMS):  $\delta$  = 8.16 (d,  $^3J(\text{H,H})$  = 8.2 Hz, 2H), 7.90 (d,  $^3J(\text{H,H})$  = 8.7 Hz, 2H), 7.86 (d,  $^3J(\text{H,H})$  = 8.2 Hz, 4H), 7.56 (d,  $^3J(\text{H,H})$  = 8.2 Hz, 4H), 7.54 (d,  $^3J(\text{H,H})$  = 8.2 Hz, 4H), 7.46 (d,  $^3J(\text{H,H})$  = 8.7 Hz, 4H), 7.27 (d,  $^3J(\text{H,H})$  = 8.7 Hz, 4H), 7.21 (d,  $^3J(\text{H,H})$  = 8.7 Hz, 2H), 3.95 (s, 3H;  $-\text{CO}_2\text{CH}_3$ ), 1.37 ppm (s, 18H; *-t*Bu);  $^{13}\text{C}$  NMR (75 MHz,  $\text{CDCl}_3$ , TMS):  $\delta$  = 166.8, 159.8, 155.7, 150.3, 147.3, 145.7, 137.6, 137.2, 131.1, 130.7, 128.2, 126.6, 125.95, 125.92, 124.9, 122.4, 121.6, 52.4, 34.7, 31.5 ppm; UV/Vis (toluene):  $\lambda_{\text{max}}$  ( $\epsilon$ ) = 465 (17900), 330 nm ( $21\,100\text{ mol}^{-1}\text{dm}^{-3}\text{cm}^{-1}$ ); HRMS (MALDI-TOF): *m/z* calcd for  $\text{C}_{46}\text{H}_{45}\text{N}_3\text{O}_2$  [ $M^+$ ]: 671.3512; found: 671.35063.

**Synthesis of 5-[bis(4'-tert-butylbiphenyl-4-yl)amino]-2-nitrobenzyl 4-[4-[bis(4'-tert-butylbiphenyl-4-yl)amino]phenylazo]benzoate (15):** A solution of acid **13** (112 mg, 0.17 mmol, 1 equiv), 4-(dimethylamino)pyridinium *p*-toluenesulfonate (DPTS; 16 mg, 0.05 mmol, 0.3 equiv), diisopropylcarbodiimide (DIPC; 32 mg, 0.25 mmol, 1.5 equiv) in anhydrous dichloromethane (12 mL) was added slowly to a solution of alcohol **7** (100 mg, 0.17 mmol, 1 equiv) in dry dichloromethane (12 mL). The reaction mixture was allowed to stir at reflux overnight. Concentration under vacuum followed by silica gel column chromatography using a dichloromethane/petroleum ether mixture as an eluent from a 1:1 to 7:3 ratio afforded **15** (**azo-fluo1**) as a glassy red solid (130 mg, 60%);  $T_g$  =  $169^\circ\text{C}$ .  $^1\text{H}$  NMR (400 MHz,  $\text{CDCl}_3$ , TMS):  $\delta$  = 8.16 (d,  $^3J(\text{H,H})$  = 9.2 Hz, 1H), 7.96 (d,  $^3J(\text{H,H})$  = 8.7 Hz, 2H), 7.86 (d,  $^3J(\text{H,H})$  = 9.2 Hz, 2H), 7.75 (d,  $^3J(\text{H,H})$  = 8.7 Hz, 2H), 7.58 (d,  $^3J(\text{H,H})$  = 8.2 Hz, 4H), 7.54 (d,  $^3J(\text{H,H})$  = 8.7 Hz, 4H), 7.53 (d,  $^3J(\text{H,H})$  = 8.2 Hz, 4H), 7.49 (d,  $^3J(\text{H,H})$  = 8.2 Hz, 4H), 7.44 (d,  $^3J(\text{H,H})$  = 8.5 Hz, 4H), 7.39 (d,  $^3J(\text{H,H})$  = 8.5 Hz, 4H), 7.31 (d,  $^4J(\text{H,H})$  = 2.7 Hz, 1H), 7.28 (d,  $^3J(\text{H,H})$  = 8.7 Hz, 4H), 7.26 (d,  $^3J(\text{H,H})$  = 8.2 Hz, 4H), 7.22 (d,  $^3J(\text{H,H})$  = 9.2 Hz, 2H), 6.98 (dd,  $^3J(\text{H,H})$  = 9.2 Hz,

$^4J(\text{H,H})=2.7$  Hz, 1H), 5.81 (s, 2H;  $-\text{CH}_2\text{OCO}-$ ), 1.37 (s, 18H;  $-t\text{Bu}$ ), 1.30 ppm (s;  $-t\text{Bu}$ );  $^{13}\text{C}$  NMR (75 MHz,  $\text{CDCl}_3$ , TMS):  $\delta=165.41$ , 155.84, 152.87, 151.30, 150.61, 150.43, 147.35, 145.74, 144.22, 138.85, 138.55, 137.61, 137.32, 137.16, 135.71, 133.21, 130.61, 130.48, 128.44, 128.18, 127.89, 126.87, 126.71, 126.61, 125.92, 125.01, 122.59, 121.72, 116.97, 116.24, 64.22, 34.69, 34.64, 31.51, 31.46 ppm; UV/Vis (toluene):  $\lambda_{\text{max}}(\epsilon)=431$  (30100), 325 nm ( $48000 \text{ mol}^{-1}\text{dm}^{-3} \text{ cm}^{-1}$ ); HRMS (MALDI-TOF):  $m/z$  calcd for  $\text{C}_{84}\text{H}_{81}\text{N}_3\text{O}_4$  [ $M^+$ ]: 1223.62831; found: 1223.62815.

**Ab initio computations:** TD-DFT calculations were conducted using Becke's three-parameter hybrid functional and the correlation functional of Lee, Yang, and Parr (B3LYP) with a 6-31G(d) basis set as implemented in the Gaussian 03 package. Illustrations were obtained with GaussView 3.0.

**Steady-state and time-resolved photophysical studies:** UV-visible absorption spectra were recorded using a Varian Model Cary 5E spectrophotometer. Corrected emission spectra were obtained by using a Jobin-Yvon Inc spectrofluorimeter (Fluoromax 3) and fluorescence quantum yields in toluene determined from a solution of Coumarin 540A in EtOH ( $\Phi_f=0.38$ )<sup>[64]</sup> absorbing equally at the excitation wavelength. Fluorescence intensity decays were measured by the TCSPC method with a femtosecond laser excitation at 410 nm provided by a Spectra-Physics setup composed of a titanium-sapphire Tsunami laser pumped by a doubled YAG laser (Millennia), pumped itself by a two-laser diode array, and doubling LBO crystals. Light pulses at 820 nm were selected by opto-acoustic crystals at a repetition rate of 4 MHz, and then doubled at 410 nm. Fluorescence photons were detected at 600 nm through a monochromator by means of a Hamamatsu MCP R3809U photomultiplier, connected to a constant-fraction discriminator. The time-to-amplitude converter was from Tennelec. Pulse deconvolution was performed from the time profile of the exciting pulse recorded under the same conditions by using a Ludox solution. The fluorescence data were analyzed by a nonlinear least-squares global method using the Globals software package developed at the Laboratory for Fluorescence Dynamics at the University of Illinois at Urbana-Champaign, and fluorescence lifetime measurements.

**Photoisomerization kinetics:** Photoisomerization of the azo compounds was recorded on magnetically stirred solutions (absorbance close to 1) using as an excitation source a continuous Hg-Xe lamp (Hamamatsu LC8) equipped with a narrow bandpass filter at 485 nm (22 nm fwhm). The in situ photodynamics of the  $E \rightarrow Z$  reaction was followed by using a white light probe (Xe 75 W) and a CCD camera coupled with a spectrometer (Princeton Instruments). Back thermal reaction constant was valued from recording the absorbance change from the PSS by using a Cary 5E spectrophotometer.

**Ultrafast transient absorption spectroscopy:** The femtosecond transient absorption setup was described elsewhere. Briefly, an amplified Ti:sapphire laser system (Spectra-Physics Hurricane) equipped with two optical parametric amplifiers (OPAs) was used to produce an approximately 100 fs laser pulse train at a repetition rate of 1 kHz. The probe beam was provided by white light generated by focusing a small amount (20  $\mu\text{J}$  per pulse) of the fundamental beam (800 nm) on a sapphire plate or on a stirred 2 mm water cell. The probe beam was then focused on the sample. The transmitted light was coupled to the detectors by optical fibers. An Ocean Optics (Si, 2048 px) plug-in card diode array was used for the UV-visible region (200–1100 nm). To probe a homogeneously excited area, the pump beam was focused to an area of around 0.25  $\text{mm}^2$  and the probing area was kept to approximately 0.1  $\text{mm}^2$ . The samples used for this measurement were prepared so that the solution absorbance was about 1 in a cuvette of 1 mm thickness. To avoid accumulation of the Z isomer after each excitation pulse and ensure full recovery of the initial state, the samples were first prepared in the photostationary state upon irradiation at 485 nm using a continuous light, and kept under light during each series of pump-probe experiments. Global analysis of the transient absorption data was performed using Igor Pro (version 5.0.3). In all cases three or four exponential functions convoluted with a Gaussian function representing the instrumental response were used to fit a data set. The width of the Gaussian was fixed at the best value obtained

from the fits at single wavelengths, and its value was about 200 fs (fwhm) in all cases.

**Surface relief gratings:** A complete description of the holographic setup has been reported elsewhere.<sup>[65]</sup> Thin films were fabricated by spin-coating concentrated solutions (1 to 4 wt %) of the azo compound in chloroform, and subsequently dried under vacuum. Surface relief gratings were inscribed by means of a continuous ion argon laser working at 488 nm. Peak-to-trough amplitude was measured by atomic force microscopy working in a tapping mode (Veeco, model Explorer). Refractive index measurements were performed by ellipsometry by using a spectroscopic ellipsometer Jobin-Yvon Horiba UVISSEL-SE working from the UV to NIR range (250 to 1100 nm). Thickness measurements were independently performed by means of a Dektak 6M stylus profilometer (Veeco).

## Acknowledgements

Rémi Métivier (ENS Cachan, PPSM-UMR CNRS 8531, Cachan, France) is gratefully acknowledged for the elaboration of the numerical program for the kinetic determination of the  $E \rightarrow Z$  and  $Z \rightarrow E$  photoisomerization quantum yields for the azo compounds. We also thank Bernard Geffroy and Feng Yang (CEA IRAMIS-Ecole Polytechnique, LPCIM-UMR CNRS 7642, Palaiseau, France) for the ellipsometric measurements.

- [1] M. Suda, N. Kameyama, A. Ikegami, Y. Einaga, *J. Am. Chem. Soc.* **2009**, *131*, 865–870.
- [2] M. Suda, N. Kameyama, M. Suzuki, N. Kawamura, Y. Einaga, *Angew. Chem.* **2008**, *120*, 166–169; *Angew. Chem. Int. Ed.* **2008**, *47*, 160–163.
- [3] M. Suda, M. Nakagawa, T. Iyoda, Y. Einaga, *J. Am. Chem. Soc.* **2007**, *129*, 5538–5543.
- [4] M. Taguchi, K. Yamada, K. Suzuki, O. Sato, Y. Einaga, *Chem. Mater.* **2005**, *17*, 4554–4559.
- [5] R. Mikami, M. Taguchi, K. Yamada, K. Suzuki, O. Sato, Y. Einaga, *Angew. Chem.* **2004**, *116*, 6261–6265; *Angew. Chem. Int. Ed.* **2004**, *43*, 6135–6139.
- [6] N. Crivillers, E. Orgiu, F. Reinders, M. Mayor, P. Samori, *Adv. Mater.* **2011**, *23*, 1447–1452.
- [7] K. Smaali, S. Lenfant, S. Karpe, M. Ocafrain, P. Blanchard, D. Deresmes, S. Godey, A. Rochefort, J. Roncali, D. Vuillaume, *ACS Nano* **2010**, *4*, 2411–2421.
- [8] S. Karpe, M. Ocafrain, K. Smaali, S. Lenfant, D. Vuillaume, P. Blanchard, J. Roncali, *Chem. Commun.* **2010**, *46*, 3657–3659.
- [9] J. M. Mativetsky, G. Pace, M. Elbing, M. A. Rampi, M. Mayor, P. Samori, *J. Am. Chem. Soc.* **2008**, *130*, 9192–9193.
- [10] S. Yasuda, T. Nakamura, M. Matsumoto, H. Shigekawa, *J. Am. Chem. Soc.* **2003**, *125*, 16430–16433.
- [11] T. Ikeda, *J. Mater. Chem.* **2003**, *13*, 2037–2057.
- [12] Q. Li, L. Green, N. Venkataraman, I. Shiyonovskaya, A. Khan, A. Urbas, J. W. Doane, *J. Am. Chem. Soc.* **2007**, *129*, 12908–12909.
- [13] M. Mathews, R. S. Zola, D. K. Yang, Q. A. Li, *J. Mater. Chem.* **2011**, *21*, 2098–2103.
- [14] T. Mitsuoka, H. Sato, J. Yoshida, A. Yamagishi, Y. Einaga, *Chem. Mater.* **2006**, *18*, 3442–3447.
- [15] H. Muroph, M. Stollenwerk, V. Bressau, *Angew. Chem.* **2006**, *118*, 2068–2087; *Angew. Chem. Int. Ed.* **2006**, *45*, 2016–2035.
- [16] H. H. Rau, in *Photochromism, Molecules and Systems* (Ed.: H. B.-L. Eds: H. Dürr), Elsevier, Amsterdam **2003**, pp. 64–164.
- [17] T. Ikeda, J.-i. Mamiya, Y. Yu, *Angew. Chem.* **2007**, *119*, 512–535; *Angew. Chem. Int. Ed.* **2007**, *46*, 506–528.
- [18] M. Elbing, A. Blaszczyk, C. von Hänisch, M. Mayor, V. Ferri, C. Grave, M. A. Rampi, G. Pace, P. Samori, A. Shaporenko, M. Zharnikov, *Adv. Funct. Mater.* **2008**, *18*, 2972–2983.
- [19] H. Nakano, *ChemPhysChem* **2008**, *9*, 2174–2176.
- [20] Y. Yu, M. Nakano, T. Ikeda, *Nature* **2003**, *425*, 145.

- [21] M. Yamada, M. Kondo, J.-i. Mamiya, Y. Yu, M. Kinoshita, C. J. Barrett, T. Ikeda, *Angew. Chem.* **2008**, *120*, 5064–5066; *Angew. Chem. Int. Ed.* **2008**, *47*, 4986–4988.
- [22] S. Angelos, Y. W. Yang, N. M. Khashab, J. F. Stoddart, J. I. Zink, *J. Am. Chem. Soc.* **2009**, *131*, 11344–11345.
- [23] D. P. Ferris, Y. L. Zhao, N. M. Khashab, H. A. Khatib, J. F. Stoddart, J. I. Zink, *J. Am. Chem. Soc.* **2009**, *131*, 1686–1687.
- [24] A. A. Beharry, G. A. Woolley, *Chem. Soc. Rev.* **2011**, *40*, 4422–4437.
- [25] E. J. Harbron, D. A. Vicente, M. T. Hoyt, *J. Phys. Chem. B* **2004**, *108*, 18789–18792.
- [26] K. Kiyose, K. Hanaoka, D. Oushiki, T. Nakamura, M. Kajimura, M. Suematsu, H. Nishimatsu, T. Yamane, T. Terai, Y. Hirata, T. Nagano, *J. Am. Chem. Soc.* **2010**, *132*, 15846–15848.
- [27] S. M. Lewis, E. J. Harbron, *J. Phys. Chem. C* **2007**, *111*, 4425–4430.
- [28] M. Han, M. Hara, *J. Am. Chem. Soc.* **2005**, *127*, 10951–10955.
- [29] M. Han, D. Ishikawa, E. Muto, M. Hara, *J. Lumin.* **2009**, *129*, 1163–1168.
- [30] J. Yoshino, A. Furuta, T. Kambe, H. Itoi, N. Kano, T. Kawashima, Y. Ito, M. Asashima, *Chem. Eur. J.* **2010**, *16*, 5026–5035.
- [31] J. Yoshino, N. Kano, T. Kawashima, *Chem. Commun.* **2007**, 559–561.
- [32] S. Sando, H. Abe, E. T. Kool, *J. Am. Chem. Soc.* **2004**, *126*, 1081–1087.
- [33] J. R. Lakowicz, *Principles of Fluorescence Spectroscopy*, Springer, Singapore, **2006**, pp. 278–351.
- [34] B. Valeur, *Molecular Fluorescence: Fluorescence and Applications*, Wiley-VCH, Weinheim, **2001**, pp. 72–123.
- [35] N. Tamai, H. Miyasaka, *Chem. Rev.* **2000**, *100*, 1875–1890.
- [36] I. K. Lednev, T.-Q. Ye, R. E. Hester, J. N. Moore, *J. Phys. Chem.* **1996**, *100*, 13338–13341.
- [37] L.-H. Liu, K. Nakatani, E. Ishow, *New J. Chem.* **2009**, *33*, 1402–1408.
- [38] L.-H. Liu, K. Nakatani, R. Pansu, J.-J. Vachon, P. Tauc, E. Ishow, *Adv. Mater.* **2007**, *19*, 433–436.
- [39] K. Liang, M. S. Farahat, J. Perlstein, K.-Y. Law, D. G. Whitten, *J. Am. Chem. Soc.* **1997**, *119*, 830–831.
- [40] E. Ishow, A. Brosseau, G. Clavier, K. Nakatani, R. B. Pansu, J.-J. Vachon, P. Tauc, D. Chauvat, C. R. Mendonca, E. Piovesan, *J. Am. Chem. Soc.* **2007**, *129*, 8970–8971.
- [41] E. Ishow, A. Brosseau, G. Clavier, K. Nakatani, P. Tauc, C. Fiorini-Debuisschert, S. Neveu, O. Sandre, A. Leaustic, *Chem. Mater.* **2008**, *20*, 6597–6599.
- [42] M. A. Petti, T. J. Shepodd, R. E. Barrans, D. A. Dougherty, *J. Am. Chem. Soc.* **1988**, *110*, 6825–6840.
- [43] R. Siewertsen, H. Neumann, B. Buchheim-Stehn, R. Herges, C. Näther, F. Renth, F. Temps, *J. Am. Chem. Soc.* **2009**, *131*, 15594–15595.
- [44] R. Loucif-Saibi, K. Nakatani, J. A. Delaire, M. Dumont, Z. Sekkat, *Chem. Mater.* **1993**, *5*, 229–236.
- [45] G. Tiberio, L. Muccioli, R. Berardi, C. Zannoni, *ChemPhysChem* **2010**, *11*, 1018–1028.
- [46] G. Gabor, E. Fischer, *J. Phys. Chem.* **1971**, *75*, 581–583.
- [47] P. Sierocki, H. Maas, P. Dragut, G. Richardt, F. Vögtle, L. Cola, A. M. Brouwer, J. I. Zink, *J. Phys. Chem. B* **2006**, *110*, 24390–24398.
- [48] M. Poprawa-Smoluch, J. Baggerman, H. Zhang, H. P. A. Maas, L. De Cola, A. M. Brouwer, *J. Phys. Chem. A* **2006**, *110*, 11926–11937.
- [49] B. Schmidt, C. Sobotta, S. Malkmus, S. Laimgruber, M. Braun, W. Zinth, P. Gilch, *J. Phys. Chem. A* **2004**, *108*, 4399–4404.
- [50] C.-W. Chang, Y.-C. Lu, T.-T. Wang, E. W.-G. Diau, *J. Am. Chem. Soc.* **2004**, *126*, 10109–10118.
- [51] I. K. Lednev, T. Q. Ye, P. Matousek, M. Towrie, P. Foggi, F. V. R. Neuwahl, S. Umapathy, R. E. Hester, J. N. Moore, *Chem. Phys. Lett.* **1998**, *290*, 68–74.
- [52] L. Reynolds, J. A. Gardecki, S. J. V. Frankland, M. L. Horng, M. Maroncelli, *J. Phys. Chem.* **1996**, *100*, 10337–10354.
- [53] V. M. Farztdinov, R. Schanz, S. A. Kovalenko, N. P. Ernsting, *J. Phys. Chem. A* **2000**, *104*, 11486–11496.
- [54] J. A. Mondal, M. Sarkar, A. Samanta, H. N. Ghosh, D. K. Palit, *J. Phys. Chem. A* **2007**, *111*, 6122–6126.
- [55] Submitted results.
- [56] T. Pancur, F. Renth, F. Temps, B. Harbaum, A. Kruger, R. Herges, C. Näther, *Phys. Chem. Chem. Phys.* **2005**, *7*, 1985–1989.
- [57] W. Adam, J. N. Moorthy, W. M. Nau, J. C. Scaiano, *J. Am. Chem. Soc.* **1997**, *119*, 6749–6756.
- [58] S. Komamine, M. Fujitsuka, O. Ito, K. Moriwaki, T. Miyata, T. Ohno, *J. Phys. Chem. A* **2000**, *104*, 11497–11504.
- [59] C. Lambert, J. Schelter, T. Fiebig, D. Mank, A. Trifonov, *J. Am. Chem. Soc.* **2005**, *127*, 10600–10610.
- [60] A. Jacquart, P. Tauc, K. Nakatani, E. Ishow, *J. Mater. Chem.* **2009**, *19*, 8999–9005.
- [61] J. P. Amara, T. M. Swager, *Macromolecules* **2004**, *37*, 3068–3070.
- [62] T. M. Swager, *Acc. Chem. Res.* **2008**, *41*, 1181–1189.
- [63] A. Jacquart, P. Tauc, R. B. Pansu, E. Ishow, *Chem. Commun.* **2010**, 46, 4360–4362.
- [64] G. A. Reynolds, K. H. Drexhage, *Opt. Commun.* **1975**, *13*, 222–225.
- [65] E. Ishow, R. Camacho-Aguilera, J. Guérin, A. Brosseau, K. Nakatani, *Adv. Funct. Mater.* **2009**, *19*, 796–804.

Received: October 30, 2011  
Published online: February 9, 2012